



**HAL**  
open science

## Clay minerals as geo-thermometer: A comparative study based on high spatial resolution analyses of illite and chlorite in Gulf Coast sandstones (Texas, U.S.A.)

Franck Bourdelle, Teddy Parra, Olivier Beyssac, Christian Chopin, Olivier Vidal

### ► To cite this version:

Franck Bourdelle, Teddy Parra, Olivier Beyssac, Christian Chopin, Olivier Vidal. Clay minerals as geo-thermometer: A comparative study based on high spatial resolution analyses of illite and chlorite in Gulf Coast sandstones (Texas, U.S.A.). *The American Mineralogist*, 2013, 98 (5-6), pp.914-926. 10.2138/am.2013.4238 . hal-02270196

**HAL Id: hal-02270196**

**<https://hal.sorbonne-universite.fr/hal-02270196>**

Submitted on 23 Aug 2019

**HAL** is a multi-disciplinary open access archive for the deposit and dissemination of scientific research documents, whether they are published or not. The documents may come from teaching and research institutions in France or abroad, or from public or private research centers.

L'archive ouverte pluridisciplinaire **HAL**, est destinée au dépôt et à la diffusion de documents scientifiques de niveau recherche, publiés ou non, émanant des établissements d'enseignement et de recherche français ou étrangers, des laboratoires publics ou privés.

1 **Clay minerals as geo-thermometer: A comparative study based on high-spatial-**  
2 **resolution analyses of illite and chlorite in Gulf Coast sandstones (Texas, USA)**

3  
4 Franck Bourdelle<sup>1,2,3,\*</sup>, Teddy Parra<sup>2</sup>, Olivier Beyssac<sup>1</sup>, Christian Chopin<sup>3,†</sup>, and Olivier  
5 Vidal<sup>4</sup>

6  
7 <sup>1</sup> IMPMC, UPMC-CNRS, Campus Jussieu, Case courrier 115, 4 place Jussieu, 75005 Paris,  
8 France.

9 <sup>2</sup> IFP Energies nouvelles, 1 et 4 avenue de Bois Préau, 92852 Rueil-Malmaison cedex,  
10 France.

11 <sup>3</sup> Laboratoire de Géologie, Ecole normale supérieure - CNRS, 24 rue Lhomond, 75231 Paris  
12 cedex 5, France.

13 <sup>4</sup> CNRS, Université Joseph Fourier Grenoble, ISTERre, BP 53, 1381 rue de la piscine, 38041  
14 Grenoble Cedex, France.

15  
16 \* E-mail address: franck.bourdelle@gmail.com

17 † E-mail address: christian.chopin@ens.fr

18  
19 Abstract

20  
21 Phyllosilicates are among the most important stable minerals within the Earth's crust. Their  
22 potential use as geo-thermometer bears great potential for application to the thermal history of  
23 rocks within the stability range of layered silicates. A high-resolution analytical technique  
24 combining Focused Ion Beam (FIB) milling and Analytical Electron Microscopy (AEM)  
25 analysis has been applied to a series of sandstone core samples from the Gulf Coast (Texas,

26 USA). The nanoscale compositional variations of K-deficient mica and chlorite flakes show  
27 that rim compositions are the most likely to approach equilibrium compositions, whereas core  
28 compositions may be relict, especially for illite-like phases. These rim analyses were used to  
29 test existing empirical or thermodynamically formulated thermo(baro)meters against  
30 maximum temperatures, which are perfectly constrained for the selected samples as they were  
31 measured *in situ* during drilling (100-230°C and 300-1200 bars). The results show that most  
32 of the empirical models overestimate the temperature, while thermodynamic models yields  
33 reasonable estimates for diagenetic to anchizonal conditions, especially if the Fe<sup>3+</sup> content is  
34 taken into account. This study clearly shows that phyllosilicates thermometry is reliable when  
35 combined with an analytical technique giving access to the fine-scale compositional  
36 variations that may represent local equilibration, whereas using micrometric compositional  
37 analysis precludes trustworthy application of such thermometers.

38

39 Key-words: illite, chlorite, zonation, thermometry, diagenesis, Gulf Coast.

40

41

## Introduction

42

43 Phyllosilicates are widespread minerals in most diagenetic and low-grade  
44 metamorphic rocks. For a long time, their compositional variations have attracted interest as  
45 potential markers of diagenesis and burial conditions like temperature (*T*), pressure (*P*), rock  
46 composition, or fluid availability (e.g. Walshe 1986; Vidal and Parra 2000). These  
47 compositional variations reflect the wide possible range of a number of substitutions in  
48 phyllosilicates, e.g. di-tri-octahedral, Tschermak or Fe–Mg exchange. Establishing a  
49 quantitative link between composition and formation conditions has therefore been a long

50 pursued goal, with two main approaches: empirical calibrations and thermodynamic  
51 modelling.

52 In the empirical case, Cathelineau and Nieva (1985) and Cathelineau (1988)  
53 established a correlation between chlorite tetrahedral Al occupancy (noted <sup>IV</sup>Al) and  
54 temperature. Their empirical calibrations were subsequently refined by Kranidiotis and  
55 McLean (1987), Jowett (1991), Zang and Fyfe (1995) and Xie et al. (1997) to account for the  
56 chlorite Mg and Fe contents, which depend primarily on the bulk-rock composition. These  
57 empirical thermometers can be easily implemented, but they provide contrasted, sometimes  
58 unrealistic, temperature estimates (e.g. De Caritat et al 1993; Essene and Peacor 1995; Vidal  
59 et al 1999; Parra et al 2001). More robust thermodynamic solutions have been proposed  
60 (Helgeson et al 1978; Helgeson and Aagaard, 1985; Walshe 1986; Aagard and Jahren 1992;  
61 Hutcheon 1990; Vidal and Parra 2000; Vidal et al. 2001, 2005, 2006; Parra et al. 2002; Inoue  
62 et al. 2009; Dubacq et al. 2010), but they require knowledge of the thermodynamic properties  
63 for numerous end-members as well as solid-solution mixing parameters.

64 The aim of the present study is to compare the results of such thermometers when  
65 applied to a low-temperature, diagenetic sample series of well cores for which a direct, *in situ*  
66 physical measure of temperature and pressure is available. Indeed, most chlorite and illite  
67 thermometers were calibrated either in specific conditions, e.g. a hydrothermal system  
68 (Cathelineau and Nieva, 1985), or at relatively high temperatures that were indirectly derived  
69 from petrological data, like phase-equilibria, fluid-inclusion or vitrinite-reflectance  
70 thermometry.

71 In addition, several generations of clay minerals showing various compositions  
72 generally coexist in the same rock sample, from detrital to authigenic to metamorphic, either  
73 as discrete crystals in distinct sites, or as zoned crystals with successive overgrowths on relict  
74 cores, which may record part of the clay history. In order to be able to decipher this record in

75 spite of the small grain sizes and expectedly fine scale of the chemical features, a high spatial  
76 analytical resolution is needed. The present study takes advantage of recent developments in  
77 combining Focused Ion Beam (FIB) sectioning (e.g. Wirth 2004) and high-resolution  
78 transmission electron microscopy (TEM) with coupled energy-dispersive X-ray analysis  
79 (EDX). This combination allows both a nanometre-scale resolution of chemical variations and  
80 then a detailed investigation of the compositional (and thus crystallization temperature)  
81 evolution of phyllosilicates in 2D at the thin-section scale, as it is classically made for  
82 metamorphic rocks with electron microprobe analysis (EMPA). The coupled FIB, TEM and  
83 EDX techniques were used to explore intracrystalline compositional variations, in an attempt  
84 at identifying the compositional domains that may record equilibration at peak temperatures  
85 for the key assemblages chlorite + quartz, chlorite + illite and illite + quartz. The relevant  
86 compositions were used to test empirical thermometers and the models proposed by Walshe  
87 (1986), Vidal et al. (2005) rearranged by Vidal et al. (2006), Inoue et al. (2009) and Dubacq et  
88 al. (2010) against the measured  $T$  and  $P$  in Gulf Coast drill-core samples, considering also the  
89 possible effect of the  $\text{Fe}^{3+}/\text{Fe}^{2+}$  ratio.

90

## 91 **Samples and geological settings**

92

### 93 **Samples**

94 Thirteen samples from 9 wells were taken from conventional drill cores of the Gulf  
95 Coast area (southern Texas, USA), available at the core repository, Bureau of Economic  
96 Geology and at University of Texas at Austin (USA). They were selected on the basis of their  
97 mineral contents (presence of chlorite, illite-chlorite contacts with a grain size allowing FIB  
98 cutting), and to cover the largest range of depth and temperature conditions as possible (cf.  
99 Appendix 1).

100           The selected samples are sandstones and shales of relatively uniform mineralogy,  
101 except for the relative amount of clays and/or carbonate cement (cf. Appendix 1). Samples  
102 with low or preferably no carbonate content were chosen, to minimize modification of the  
103 activity of H<sub>2</sub>O. These samples consist mostly of quartz (> 80%), with detrital feldspars, clays  
104 (detrital and authigenic) and a minor amount of carbonates (calcite and dolomite), organic  
105 matter and pyrite. Clay minerals refer to smectite, I/S, illite, chlorite and kaolinite. The  
106 analysed chlorites are devoid of 7 Å phases, as shown by TEM.

107

### 108 **Pressure and temperature conditions: thermal history of the Gulf Coast**

109           The last major tectonic event in the Gulf Coast area was the Triassic-Early Jurassic  
110 opening of the Gulf of Mexico. Then, the southern part of Texas remained tectonically quiet  
111 throughout the Cenozoic Era (Stanley 1986; Posey 1986), with a continuous marine  
112 deposition offshore. Thus, the temperature distribution within the sediments remained similar  
113 to the classic *T*-depth burial distribution during the Cenozoic, after the thermal anomaly  
114 resulting from rifting was dissipated (Nunn 1984). The selected samples are from onshore  
115 area, resulting of recent marine regression. At depth, some thermal anomalies exist locally  
116 due to advecting fluids moving along the growth faults (Jones 1975; Bodner and Sharp 1988).  
117 These anomalies might be due to the presence of salt beds at depth, inducing heterogeneities  
118 in thermal conductivity (Bodner 1985), and from a thermal anomaly of the lithosphere  
119 (Bodner 1985). However, these thermal anomalies do not affect significantly the eastern area  
120 (Frio/Vicksburg fault zone; Pfeiffer 1989). As a consequence, we assume that the present-day  
121 *P-T* conditions are the maximum temperatures and maximum pressures reached by each of  
122 the samples since its deposition. This assumption was made previously by several equivalent  
123 studies (e.g. Hillier and Velde, 1991) and is supported by (i) the regular subsidence and a  
124 continuous sediment deposition (Royden et al 1980) during the Cretaceous and the Cenozoic



150 Cappellen and Doukhan 1994; Bourdelle et al. 2012). Twenty-three FIB thin sections were  
151 cut from 12 samples, across illite-chlorite contacts near the end of the interface, where  
152 recrystallisation is the most likely. The thin foils were cut out with a size of approximately 15  
153  $\mu\text{m}$  by 5  $\mu\text{m}$  and a thickness between 50 and 300 nm. To check for the preservation of the  
154 minerals' crystalline structure after FIB-milling, lattice-fringe imaging was then  
155 systematically carried out with the TEM.

156 The FIB sections were analyzed with a TEM-EDX JEOL 2100-F at the Physics and  
157 Microanalysis Department of IFPEN (France), using a 200 kV voltage, a counting time of 60  
158 s and a dead time lower than 15%. The current density was maintained at 1.3 pA/cm<sup>2</sup>. The  
159 sample tilt angle was 7°. Under these conditions, the spot size was around 1 nm and could be  
160 defocused to 50 nm. The EDX analyzer was calibrated on paragonite (Na, Al), pyrophyllite  
161 (Al), talc (Mg), muscovite (Fe, Al, K), chlorite (Fe, Al), clintonite (Mg, Ca, Al) and phengite  
162 (Mg, Fe, K, Al) and the standardizations were checked against EMP analyses of reference  
163 clays (SMB-18; Kohler et al. 2009). Given the high spatial resolution, the analysis points  
164 were targeted to reveal within-grain compositional variations (Fig. 1) and, in the case of  
165 coexisting chlorite and mica, so as to obtain couples of analyses that may record local  
166 equilibrium under changing *P-T* conditions.

167 The structural formulae were calculated on the basis of 11 and 14 oxygens for illite-  
168 like phases and chlorites, respectively, with K, Na and Ca assigned to the interlayer. Several  
169 numerical criteria were applied to exclude poor-quality and/or contaminated analyses. For  
170 illite-like phases, analyses with either  $\text{K} + \text{Na} + \text{Ca} > 1$  apfu,  $\text{Si} < 3$  apfu or  $\text{Si} > 4$  apfu were  
171 excluded. For chlorites, analyses with  $\text{K}_2\text{O} + \text{Na}_2\text{O} + \text{CaO} > 1$  wt% (of the 100 wt% total of  
172 TEM-EDX analyses) were excluded.

173



174 **Intracrystalline chemical variations: interpretation and implication for**  
175 **thermobarometry**

176

177 From the high-spatial resolution dataset yielded by the analytical protocol, analyses  
178 were separated into two categories: crystal rim analyses performed at 50 nm of illite-chlorite  
179 contacts, and crystal-core analyses (Fig. 1). The comparison of core and rim analyses of illite  
180 and chlorite in the selected Gulf Coast samples reveals some systematic trends as a function  
181 of measured temperature (i.e. BHT). All the analyses obtained for 2:1 phyllosilicates show K  
182 as the dominant interlayer cation, with only traces of Na and Ca. From these observations,  
183 Figure 2 presents the K contents of 2:1 phyllosilicates vs measured temperature. In the grain  
184 cores of each sample, the K content ranges between ~0.5 and 0.8 to 0.98 apfu regardless of  
185 the temperature attained (examples of illite rims analyses in Table 1; cf. Appendix 2). In  
186 contrast, the maximum K content of the rim analyses increases from ~0.4-0.5 apfu (at ~100  
187 °C) to 0.7-0.9 apfu (at ~230 °C), which reflects the compositional evolution due to illitization  
188 (e.g. Perry and Hower 1970; Cathelineau and Nieva 1985; Mathieu and Velde 1989; Lanson  
189 and Besson 1992; Battaglia 2004). The rim compositions with maximum K were thus  
190 considered to be the compositions closest to equilibrium compositions. Conversely, the K-rich  
191 core analyses obtained in the low- $T$  samples most likely reflect inherited compositions of  
192 detrital material and were not considered further for thermometry. In contrast to the  
193 temperature-dependence of the K content,  $^{VI}Al$  (between 1.5 and 2 apfu), Fe + Mg (about 0.6  
194 apfu) contents and XFe ( $0.5 \pm 0.1$ ) show no evolution with temperature for the rim  
195 compositions. A variation with  $T$  of Si content is observable, but not obvious to decipher. The  
196 observed trend in K content (Fig. 2) and the possible trend in Si (or  $^{IV}Al$ ) content with  
197 temperature are accounted for by the combination of the pyrophyllitic ( $^{IV}Si^{XII}\square = ^{IV}Al^{XII}K$ )  
198 and Tschermak substitutions ( $^{IV}Si^{VI}(Fe, Mg) = ^{IV}Al^{VI}Al$ ), or any linear combination of them

199 like  ${}^{\text{VI}}\text{Al}^{\text{XII}}\square = {}^{\text{VI}}\text{Fe}^{\text{XII}}\text{K}$  (i.e. octahedral-interlayer exchange), where IV, VI and XII identify  
200 tetrahedral, octahedral and interlayer sites respectively, and  $\square$  represents octahedral  
201 vacancies. According to the observed K contents, we are dealing with illite or K-smectite,  
202 simply referred to as illite or K-deficient mica in the following since the thermometers tested  
203 consider them collectively.

204         The tetrahedral Al content ( ${}^{\text{IV}}\text{Al}$ ) of core and rim chlorite grains shows a rough  
205 increase with  $T$ , as expected from earlier studies (Fig. 3). More surprising is the consistently  
206 (except at 129 and 191 °C) higher  ${}^{\text{IV}}\text{Al}$  maximum value in core than in rim, which is opposite  
207 to the trend documented by e.g. Jahren (1991), in zoned authigenic chlorite crystals of the  
208 North Sea. This feature suggests that some crystal cores may be of dedrital origin and have  
209 retained the high  ${}^{\text{IV}}\text{Al}$  content typical for metamorphic chlorites, with their inherent  
210 variability. For this reason, only the rim compositions of chlorite were considered for  
211 thermometry (examples of chlorite rims analyses are given Table 2 and Appendix 3). In  
212 details, these rim compositions of the Gulf Coast chlorites vary with temperature similarly to  
213 that reported in previous studies on diagenetic clays (e.g. Velde and Medhioub 1988; Hillier  
214 and Velde 1991; Jahren and Aagaard 1989; Jahren 1991; Jahren and Aagaard 1992), with the  
215 maximum  $\text{Al}_{\text{total}}$  and  ${}^{\text{IV}}\text{Al}$  (mirrored by Si counter-variation) contents both showing an  
216 increase with temperature (Fig. 3). The linear evolution of maximum  ${}^{\text{IV}}\text{Al}$  with temperature is  
217 from  $\sim 0.95\text{-}1.0$  apfu at 100 °C to  $\sim 1.38\text{-}1.4$  apfu at 216 °C (Fig. 3). On the contrary,  ${}^{\text{VI}}\text{Al}$   
218 shows no systematic evolution. Another obvious feature is the apparent decrease of octahedral  
219 vacancies with increasing temperature. This increase of trioctahedral character with  $T$  is a  
220 classical feature (e.g. Cathelineau 1988; Inoue et al. 2009), which suggests that, for each  
221 measured temperature, those analyses with the highest octahedral occupancy represent the  
222 closest approach to the relevant equilibrium composition (as do highest- ${}^{\text{IV}}\text{Al}$  analyses, Table  
223 2). The “equilibrium” vacancy number is then observed to decrease from 0.3 apfu at 102 °C to

224 0.1 apfu at 232 °C. In contrast, no clear trend of the Fe + Mg content and XFe evolution with  
225 temperature is apparent. The compositional variations of chlorite discussed above can be  
226 explained by a combination of the Tschermak ( ${}^{\text{IV}}\text{Si}{}^{\text{VI}}\text{R}^{2+} = {}^{\text{IV}}\text{Al}{}^{\text{VI}}\text{Al}$ ) and di-trioctahedral  
227 substitutions ( $2 {}^{\text{VI}}\text{Al}{}^{\text{VI}}\square = 3 {}^{\text{VI}}\text{R}^{2+}$ ), where  $\square$  and  $\text{R}^{2+}$  represent octahedral vacancies and  
228 divalent cations like Fe and Mg, respectively. Their combination in a 2 to 1 ratio would  
229 account for the observed variations in  ${}^{\text{IV}}\text{Si}$ ,  ${}^{\text{IV}}\text{Al}$  and vacancy, for the near constancy of  ${}^{\text{VI}}\text{Al}$ ,  
230 and slight possible increase in  $\text{R}^{2+}$ . For the two samples at 204 and 232 °C, the  ${}^{\text{IV}}\text{Al}$  and  ${}^{\text{VI}}\text{Al}$   
231 contents are surprisingly low compared to the general tendency (Fig. 3 and Table 2), and are  
232 compensated by large  $\text{R}^{2+}$  and Si contents. This may be due to a different precursor mineral, a  
233 different bulk composition, an Al-poor rock composition or a non-equilibrated mineral  
234 chemistry.

235         From these observations, the chemical variations with  $T$  and the differences between  
236 crystal core and rim compositions (Fig. 1, 2 and 3) are clearly established at the nanoscale,  
237 suggesting a chemical zonation of these phyllosilicates. This zonation can be the result of the  
238 dissolution-reprecipitation process occurring along the crystal rims, in accordance to the  $P$ - $T$   
239 conditions, in spite of the low- $T$  nature of these phyllosilicates. In addition, the scattering in  
240 the dataset observed at each temperature among the crystal-rim compositions (Fig. 2 and 3),  
241 for both illite and chlorite, suggests that rim compositions do not all record the last, highest-  
242 temperature equilibrium conditions, but that some of them were acquired during earlier stages  
243 of equilibration during burial. Indeed, each rim composition refers to a specific part of the  $P$ - $T$   
244 history of the crystal, i.e. the different compositions indicate the different steps of  
245 crystallisation with  $T$  during the burial. As a consequence, only the “extreme” compositions  
246 refer to the BHT-BHP. Owing to the difficulty to locate the rim areas that record the last and  
247 higher-temperature equilibration, we have considered only the three or four analyses (when it  
248 was possible), for each sample, that represent the compositions closest to equilibrium

249 compositions. This selection of such illite and chlorite rim analyses was used to test the  
250 phyllosilicate-based thermobarometers.

251

## 252 **Tested thermobarometers**

253

### 254 **Chlorite thermobarometry**

255 The pioneer chlorite thermometer proposed by Cathelineau and Nieva (1985) and  
256 refined by Cathelineau (1988) is an empirical calibration based on a linear increase of <sup>IV</sup>Al  
257 content with temperature. Several authors (e.g. Shau et al. 1990; De Caritat et al. 1993; Jiang  
258 et al. 1994; Essene and Peacor 1995) have criticized the use of this equation as a thermometer,  
259 firstly because the chlorite analyses used for the equation calibration were suspected to be  
260 contaminated by other mineral phases, and secondly because the <sup>IV</sup>Al content of chlorite also  
261 depends on the bulk-rock composition. The latter point implies that the thermometer should  
262 not been used for other rock composition than the one used for its calibration. In order to take  
263 bulk-rock composition effects into account, several tentative corrections were introduced in  
264 various empirical equations, mainly based on the Fe/(Fe+Mg) ratio (Kranidiotis and McLean  
265 1987; Jowett 1991; Hillier and Velde 1991; Zang and Fyfe 1995; Xie et al. 1997). All these  
266 equations are tested in this study and summarized in Table 3 and Appendix 4.

267 Alternatively, thermodynamic or semi-thermodynamic models were proposed by Walshe  
268 (1986), Vidal et al. (2005, 2006) and Inoue et al. (2009), to estimate *P-T* formation conditions  
269 from chlorite compositions, in most instances considering the chlorite+quartz equilibrium.  
270 These models differ by the choice of the end-member components and activity-composition  
271 relationships, and by the *P-T* data used to constrain the activity models (cf. Appendix 4).  
272 Moreover, Walshe (1986) and Inoue et al. (2009) neglected the non-ideal contributions and  
273 the effect of pressure, whereas Vidal et al. (2005) took them into account. According to the

274 chlorite structure (Bailey 1988; Holland et al. 1998), two assumptions are also possible for the  
275 cationic mixing model: an ordered distribution, which was adopted by Vidal et al. (2005,  
276 2006), or a random mixing, as used by Walshe (1986) and Inoue et al. (2009) (Table 3). In  
277 order to test these models, we assumed that  $a_{\text{qz}} = 1$  and  $a_{\text{H}_2\text{O}} = 1$ , which is ensured by the  
278 presence of quartz and seems reasonable for low- $T$  chlorite of diagenetic and hydrothermal  
279 origin (Inoue et al. 2009), and accounts for the low carbonate content in the rocks. In addition,  
280 and contrary to the empirical thermometers, these three thermodynamic models require an  
281  $\text{Fe}^{3+}$  content estimate to be applied. In this study,  $\text{Fe}^{3+}/\Sigma\text{Fe}$  ratios were estimated by the multi-  
282 equilibrium approach of Vidal et al. (2006).

283

#### 284 **K-deficient mica thermobarometry**

285 Battaglia (2004) proposed an empirical illite thermometer directly based on K content  
286 with a correction accounting for the Fe-Mg content, which is considered as an indicator of the  
287 variation of rock composition. Besides, Parra et al. (2002) proposed and calibrated a  
288 thermodynamic model representing the phengite-quartz equilibrium, calculated from activity  
289 of chosen end-members and taking into account the non-ideal part of activity coefficients.  
290 Dubacq et al. (2010) extended this model to smectite, illite, interlayered smectite-illite and  
291 mica by considering the  $T$ -hydration relationship, the pressure and the rock composition, and  
292 using multi-equilibrium thermobarometry. This model was the first attempt to provide a  
293 unique set of 2:1 phyllosilicates thermodynamic properties in a solid-solution model relevant  
294 from diagenetic to metamorphic conditions. The model involves an assumed ordered cationic  
295 distribution and nine end-members (one of which has several levels of hydration), in order to  
296 cover the whole compositional space of 2:1 phyllosilicates (cf. Appendices 1 and 3). The  
297 Dubacq et al. (2010) model also considers the non-ideality of cationic exchanges and, on the  
298 basis of three independent equilibria and their hydrated equivalent for any smectite, illite or

299 mica + quartz + water equilibrium, yields a pressure–temperature relation simultaneously with  
300 the hydration state (Table 3).

301

### 302 **Illite-chlorite assemblages**

303         With the high-spatial-resolution analytical protocol used in this study, we can target  
304 pairing of illite and chlorite analyses supposed to represent local equilibria. The relevant  
305 heterogeneous equilibrium was envisaged by Walshe (1986) as a thermometer, considering a  
306 chlorite + mica + quartz + K-feldspar + water assemblage. The author chose to represent the  
307 mica phase with a muscovite structure and a random-mixing cation distribution and ideal  
308 activities (cf. Appendix 4). This equilibrium was also used to justify the combination of Vidal  
309 et al. (2005, 2006) and Dubacq et al. (2010) models as a multi-equilibrium approach. In this  
310 case, the non-ideal ordered models for illite-micas (Dubacq et al. 2010) and chlorites (Vidal et  
311 al. 2005, 2006) can be used simultaneously to deduce  $T$  and  $P$ , assuming the achievement of  
312 local equilibrium between chlorites and illites. This is what has been tested and applied in this  
313 study to a series of Gulf Coast samples and summarized in Table 3.

314

### 315 **$P$ - $T$ estimates from Gulf Coast phyllosilicates**

316

#### 317 **Estimation of $Fe^{3+}/\Sigma Fe$ used to test thermobarometers**

318         The chlorite thermodynamic thermobarometers need an estimation of  $Fe^{3+}/\Sigma Fe$  ratios  
319 to be correctly applied. However, measuring the  $Fe^{3+}$  content at the nanoscale is challenging,  
320 even with the recent methods. For instance, the scanning transmission X-ray microscopy  
321 (STXM) and X-ray absorption near edge-structure (XANES) study of Bourdelle (2011, *PhD*)  
322 on Gulf Coast chlorites remains only qualitative. In order to circumvent the  $Fe^{3+}$  issue, Vidal  
323 et al. (2005) and Vidal et al. (2006) proposed a numerical method to estimate a minimum

324  $X_{Fe^{3+}} = Fe^{3+}/\Sigma Fe$  based on the achievement of convergence of 4 reactions (chlorite+quartz  
325 and internal chlorite equilibria) at a given pressure, and a maximum  $X_{Fe^{3+}}$  when the  
326 equilibrium convergence is lost. Vidal et al. (2006) have shown on millimetre-size chlorites  
327 that the minimum  $Fe^{3+}$  content calculated in this way was compatible with XANES  
328 measurements and can be used as an approximation of the actual  $Fe^{3+}$  content. Moreover, the  
329 difference between estimates of the minimum and maximum  $X_{Fe^{3+}}$  ratios is small in the low-  
330  $T$  contexts. Therefore, we used the multi-equilibrium method proposed by Vidal et al. (2005,  
331 2006) to estimate the  $Fe^{3+}/\Sigma Fe$  ratio in Gulf Coast chlorites and used the results as input  
332 values in Vidal et al. (2005, 2006), Inoue et al. (2009) and Walshe (1986) models (where  $Fe^{3+}$   
333 replaces  $^{VI}Al$ ). This estimated minimum  $Fe^{3+}/\Sigma Fe$  was found to range between 0.1 and 0.45,  
334 which seems realistic for low- $T$  chlorites (e.g. Inoue et al. 2009) and in agreement with  
335 literature data and our STXM-XANES qualitative study (Bourdelle 2011, *PhD*). We assumed  
336 that the  $Si > 3$  apfu analyses, which are excluded by the models of Vidal et al. (2005) and  
337 Vidal et al. (2006), have the same  $X_{Fe^{3+}}$  ratio as the Si-poor analyses of the same sample.  
338 This assumption is supported by the consistency of the minimum  $X_{Fe^{3+}}$  values obtained for  
339 all the analyses ( $Si < 3$  apfu) of any given sample. Even if these  $X_{Fe^{3+}}$  estimates are fraught  
340 with uncertainties, their input in the  $T$  calculations allows a sensitivity test of the various  
341 models with respect to  $X_{Fe^{3+}}$ .

342         Regarding the illite case, we do not have a numerical method to estimate the  $Fe^{3+}$   
343 content. However, the qualitative XANES study of Bourdelle (2011, *PhD*) showed that 2:1  
344 phyllosilicates of the Gulf Coast have a  $Fe^{3+}/(Fe^{3+} + Fe^{2+})$  ratio higher than 50%. Because  
345 taking ferric iron into account implies an increase of calculated vacancies, the sensitivity of  
346 Dubacq et al. (2010) model to the  $X_{Fe^{3+}}$  had to be tested. This model was therefore applied to  
347 Gulf Coast illite under two limiting assumptions, with  $X_{Fe^{3+}} = 0$  (case 1) and  $X_{Fe^{3+}} = 0.7$   
348 (case 2).

349

## 350 **Results from Gulf Coast chlorites**

351           In order to test the available chlorite thermometers, we have selected for each present-  
352 day  $P$  and  $T$  values only the three or four analyses that represent the closest approach to the  
353 relevant equilibrium composition, referred to as “maximum zoning composition”. For the  
354 empirical thermometers, these are the highest-<sup>IV</sup>Al analyses; for thermodynamic models, these  
355 are the extremum  $\log K$  analyses (with > 80% overlap between the two sets), depending on  
356 the direction of the reaction.

357           The application of all the *empirical* chlorite thermometers according to measured  
358 temperature for the Gulf Coast samples shows that calculated  $T$  are systematically  
359 overestimated with respect to measured  $T$ . The thermometers of Cathelineau (1988),  
360 Kranidiotis and McLean (1987), Jowett (1991) and Xie et al. (1997) predict a maximum  
361 temperature of  $360 \pm 20$  °C for the measured temperature of 216 °C. These four different  
362 chlorite thermometers give similar results, showing the weak impact of the XFe corrections in  
363 the equations. Using the Zang and Fyfe (1995) equation, in which XFe has a stronger  
364 influence on the temperature estimation, the calculated temperatures are closer to measured  
365 temperatures, but still too high, e.g. 286 °C for a measured temperature of 216 °C. Hillier and  
366 Velde (1991) equation gives the closest, but the most scattered, temperature estimates to  
367 measured temperature, with results between 75 and 380 °C. Interestingly, their calibration is  
368 the only one that includes Gulf Coast chlorites (for which they pointed out the high <sup>IV</sup>Al  
369 content).

370           Temperature estimations obtained with the *thermodynamic* models of Walshe (1986),  
371 Inoue et al. (2009) and Vidal et al. (2005, 2006) models are represented on Figure 4, with all  
372 iron considered as Fe<sup>2+</sup> (case 1) and with Fe<sup>3+</sup> as obtained with the Vidal et al. (2005, 2006)  
373 convergence method and assumed to replace <sup>VI</sup>Al (case 2).



374 In the case of  $\text{Fe}_{\text{total}} = \text{Fe}^{2+}$ , all the thermometers overestimate temperatures. The Walshe  
375 (1986) thermometer gives a temperature trend between 205 °C and 323 °C for present-day  
376 temperatures of 102 °C and 216 °C, respectively. Although the results obtained for samples at  
377 204 °C and 232 °C are out of the general trend, this model overestimates systematically  
378 temperatures by an average of ~70 °C — and excludes many Si-poor analyses ( $\text{Si} < 3$  apfu)  
379 due to inappropriate choice of end-members. The results obtained with the Inoue et al. (2009)  
380 method show a systematic trend of  $T$  overestimation by ~40 °C on the low- $T$  side to ~70 °C  
381 on the high- $T$  side (Fig. 4). The model of Vidal et al. (2005, 2006), which excludes many  
382 analyses ( $\text{Si} > 3$  apfu), gives more scattered results but these are in better agreement with  
383 measured temperatures and distributed on either side of the 1:1 line, with an average deviation  
384 between calculated temperatures and BHT of 7 °C, against 65 °C and 59 °C for Inoue et al.  
385 (2009) and Walshe (1986) models, respectively.

386 Taking into account the  $\text{Fe}^{3+}$  content, all thermodynamic models give lower or less  
387 dispersed temperatures (Fig. 4). Regarding the Vidal et al. (2005, 2006) model, the most  
388 visible effect of the ferric iron is the narrowing of the data scatter. The calculated  $T$  values  
389 decrease compared to the same dataset without  $\text{Fe}^{3+}$  content when they are higher than 150  
390 °C, and increase when they are below 150 °C. These trends were also noticed by Inoue et al.  
391 (2009) as they tested the effect of  $\text{Fe}^{3+}$  on the Vidal et al. (2001) model. Temperatures  
392 calculated with the Walshe (1986) model are slightly but consistently lower when a minimum  
393  $\text{Fe}^{3+}$  content is considered, by about 15 °C on average. Maximum calculated temperatures  
394 range from 190 °C to 308 °C for the present-day temperatures of 102 °C to 216 °C,  
395 respectively. The  $\text{Fe}^{3+}$  content has a limited effect and the temperature overestimation  
396 persists. In the same way, the results given by the thermometer of Inoue et al. (2009) are  
397 systematically lower when  $\text{Fe}^{3+}$  content is considered, by about 20 °C on average, even if for a  
398 few analyses the shift can be as large as 100 °C ( $X_{\text{Fe}^{3+}} = 0.3$ ). New temperatures remain

399 overestimated for most of them, for instance they spread between 140°C and 181°C for a  
400 measured  $T$  of 102 °C, between 134 °C and 285 °C for a measured  $T$  of 191 °C, and between  
401 261 °C and 325 °C for a measured  $T$  of 216 °C.

402

### 403 **Results from Gulf Coast K-deficient micas**

404 As for chlorite, the available illite thermometers were tested using only the three or  
405 four analyses that may be the closest to the “maximum zoning composition” for each present-  
406 day  $P$  and  $T$ . For the empirical thermometers, these are the highest-K analyses; for  
407 thermodynamic models, these are the extremum  $\log K$  analyses (with > 85% overlap between  
408 the two sets), depending on the direction of reaction.

409 The empirical illite thermometer (Battaglia, 2004) gives results that show a positive  
410 correlation with the measured temperatures (Fig. 5), but with a systematic shift by an average  
411 of about +40-50 °C at high  $T$  and about +60-70 °C at low  $T$ .

412 The thermodynamic model of Dubacq et al. (2010) yields for each analysis of illite in  
413 equilibrium with quartz a  $P$ - $T$ - $m\text{H}_2\text{O}$  stability relation. In the present case, the measured  
414 pressure was used as input value to calculate the temperature and hydration state. The results  
415 obtained with  $\text{Fe}_{\text{total}} = \text{Fe}^{2+}$  (Fig. 6) show that most calculated temperatures are slightly  
416 overestimated (by less than 50 °C) and are less well correlated with measured  $T$  than with the  
417 Battaglia (2004) thermometer. Maximum temperatures range from 165 °C to 256 °C for  
418 measured 121 °C and 216 °C respectively, and 230 °C for measured 232 °C. If the  
419 calculations are made assuming  $X\text{Fe}^{3+} = 0.7$  on the basis of preliminary STXM-XANES data,  
420 the results show (Fig. 6) a very similar pattern of overestimation, but with a slightly wider  
421 data scattering than with pure  $\text{Fe}^{2+}$ .

422

### 423 **Results from illite-chlorite assemblages**

424 To use illite + chlorite thermometers, three or four illite-chlorite pairs of rim analyses,  
425 located at less than 50 nm on either side of the illite-chlorite interface, were retained for each  
426 sample, whenever possible. When testing the effect of ferric iron, we used the same input data  
427 as above, i.e.  $X_{\text{Fe}^{3+}}$  ratio varying between 0.1 and 0.45 in chlorite as obtained with the Vidal  
428 et al. (2005, 2006) method, and the fixed value of 0.7 in illite-like phases according to STXM-  
429 XANES results.

430 In the case of the Walshe (1986) method,  $\log K$  is negatively correlated with  
431 temperature, and the selected pairs are those yielding the lowest  $\log K$  values. The reaction  
432 involved in the Walshe (1986) calculation requires the presence of K-feldspar in the  
433 assemblage, which was observed by SEM in most of our samples. The resulting calculated  
434 temperatures show a positive correlation with the measured temperatures (Fig. 7), provided  
435 the 102 °C sample is considered as an outlier, but they are generally overestimated by ~0-60  
436 °C. Results show a trend between 133-172 °C for a measured 121 °C to 272-320 °C for a  
437 measured 232 °C. The  $\text{Fe}^{3+}$  content has no effect as the corresponding temperatures differ  
438 from the previous ones by only 3 to 4 °C.

439 The results of the multi-equilibrium calculation based on Vidal et al. (2005, 2006)  
440 model and Dubacq et al. (2010) hydration model are shown in Figure 8. As consideration of  
441  $\text{Fe}^{3+}$  was shown to hardly improve chlorite thermometry and to slightly affect illite  
442 thermometry with these database and solution models, only calculations with minimum  $X_{\text{Fe}^{3+}}$   
443 are presented here. Unlike most other models, the calculated temperatures (calculation from  
444 BHP; Fig. 8-b) are not clearly overestimated, but are within  $\pm 50$  °C of the measured  
445 temperatures. In contrast, the calculated pressures (Fig. 8-c) are not reliable, as they  
446 sometimes exceed 5 kbar, for a maximum measured value of 1.2 kbar.

447

448

## Discussion

449

450 **The need for spatially highly resolved analyses and relevant analyses selection for clay**  
451 **thermometry**

452         The fine-scale compositional variations of low-*T* chlorites and illites were studied on  
453 diagenetic crystals as a function of increasing *P-T* conditions with a very high spatial control  
454 on microtextural interactions. Using this protocol, the presence of an intra-crystalline  
455 chemical zonation in low-*T* crystals was clearly established. The composition of the grain  
456 rims seems to respond to the *P-T* variations and therefore to approach equilibrium while the  
457 crystal core may preserve relic compositions. However, the dispersion at each temperature of  
458 crystal-rim compositions, for both illite and chlorite, indicates that rim compositions do not  
459 all record the last, highest-temperature equilibrium conditions but that some of them were  
460 acquired during earlier stages of equilibration during burial. Thus, the selection of analyses  
461 becomes a crucial point when trying to estimate the formation temperature and thermometry  
462 is not straightforward because the composition of each part of a crystal may refer to one part  
463 of the *P-T*/burial history. Using EMP would lead to average the crystal core-rim  
464 compositions, and to a biased application of geothermobarometers. In this way, it is clear that  
465 the use of TEM, with high spatial resolution, is highly recommended.

466

467 **Evaluation of clay minerals thermometry and Fe<sup>3+</sup> effect**

468         In the chlorite case, the empirical approaches based on the aluminum content  
469 (Cathelineau 1988; Kranidiotis and McLean 1987; Jowett 1991; Hillier and Velde 1991; Zang  
470 and Fyfe 1995; Xie et al. 1997) give disparate temperatures and overestimate the temperature  
471 of our Gulf Coast samples by up to 170°C with respect to BHT, taken as indicative of the  
472 maximum burial conditions insofar as the subsidence has been continuous since the  
473 Cretaceous. In contrast, the temperature estimated with the models of Vidal et al. (2005,

474 2006) and Inoue et al. (2009) [as well as the chlorite + mica + K-feldspar + quartz + water  
475 equilibrium of Walshe (1986)] are in fair agreement with the BHT. This difference in the  
476 results between empirical calibrations and thermodynamic approaches suggests that empirical  
477 chlorite thermometers are inaccurate, most likely because of their inability to account properly  
478 for bulk-rock compositional effects. This conclusion is in line with the results of earlier  
479 studies by De Caritat et al. (1993) and Essene and Peacor (1995), which concluded that the  
480 empirical thermometers based on the <sup>IV</sup>Al content of chlorite are inaccurate and should be  
481 used with caution. In this context, the use of a spatially highly resolved analytical approach  
482 cannot help to improve the results.

483         The temperatures estimated from chlorite compositions with the non-empirical  
484 thermodynamic approach of Vidal et al. (2005, 2006) are in better agreement with the BHT,  
485 but the calculated temperatures are slightly scattered. Moreover, the numerous chlorite  
486 analyses showing high Si content (> 3 apfu) cannot be handled with this model. The semi-  
487 empirical approaches proposed by Walshe (1986) and especially by Inoue (2009) yield  
488 temperature estimates higher than but still in reasonable agreement with the BHT. As in the  
489 case of Vidal et al. (2005, 2006) model, the Walshe (1986) formalism cannot handle all the  
490 chlorite compositions measured in our samples, and is limited to chlorite with Si > 3 pfu.  
491 Only the formalism of Inoue et al. (2009) can be used for the entire set of compositions  
492 measured for Gulf Coast samples.

493         The present study also shows the strong effect of the distinction between Fe<sup>3+</sup> and Fe<sup>2+</sup>  
494 (Fig. 4) and confirms previous observations (Vidal et al. 2006; Inoue et al. 2009). The  
495 consideration of Fe<sup>3+</sup> content increases the number of octahedral vacancies and reduces the  
496 R<sup>2+</sup> occupancy. As octahedral vacancy (sidoite content and activity) is negatively correlated  
497 with *T*, the reduced R<sup>2+</sup> occupancy generally results in a lower calculated temperature.  
498 However, the temperature variation due to the introduction of Fe<sup>3+</sup> content is different for

499 each thermometer. Inoue et al. (2009) model is the most sensitive to ferric iron (Fig. 4), with a  
500  $T$  variation between cases 1 and 2 ranging from 7 to 108 °C, compared to 6-49 °C for Walshe  
501 (1986) model and 0-59 °C for Vidal et al. (2005; 2006) model (Fig. 4). The choice of a  
502 random-mixing repartition of cations in the model of Inoue et al. (2009) seems to be the  
503 reason for this difference, because the vacancy number has a greater weight in the  $\log K$   
504 calculation of random-mixing models than in the ordered model. Surprisingly, the Vidal et al.  
505 (2005, 2006) model is the only one for which  $\text{Fe}^{3+}$  consideration increases the calculated  
506 temperatures at low- $T$  and decreases them at high- $T$ . In summary, all the thermodynamic  
507 models give overestimated and scattered temperatures if all iron is assumed as ferrous; taking  
508 into account a minimum  $\text{Fe}^{3+}$  occupancy leads to reduce the overestimation, whereas the  
509 results still remain slightly scattered. The valence state of iron is therefore not the sole reason  
510 for the inaccuracy of chlorite thermodynamic thermometers.

511 The observed scatter of results can be due to some errors, which stem from the uncertainties  
512 in BHT, in the thermodynamic standard-state properties of the end-members and solution  
513 models, departure of the analysed compositions from equilibrium compositions, and  
514 analytical uncertainties. The source of error resulting from the uncertainties associated with  
515 the thermodynamic data is difficult to estimate, because the thermodynamic data used for  
516 example by Vidal et al. (2005, 2006) model were calibrated using experimental and natural  
517 data of various levels of confidence. However, it is likely that the uncertainties in the  
518 thermodynamic data have a systematic effect on the calculated locations of the  
519 chlorite+quartz equilibrium. Moreover, the uncertainties in the thermodynamic data cannot be  
520 put forward in the case of Inoue et al. (2009) model, which is semi-empirical and not based on  
521 thermodynamic properties.

522 Even if the thermodynamic data were perfect, imprecision in the analysed compositions of  
523 minerals places limits on the accuracy with which  $T$  can be known. The scatter resulting from

524 the variation of the chlorite compositions within specific bounds given by the precision of the  
525 TEM analysis (element-dependent) can be calculated with a Monte Carlo technique  
526 (Lieberman and Petrakakis 1991). Thus, the effect of analytical uncertainties was simulated  
527 (i) to confirm that the observed compositional variations are significant and not due to the  
528 inaccuracy of analyses and (ii) to compare the accuracy of each thermometer by the  
529 evaluation of the sensitivity of the equilibrium  $K$  constant calculation to a slight variation of  
530 composition. In this MonteCarlo study, we focussed on the chlorite models of Walshe (1986),  
531 Vidal et al. (2005, 2006) and Inoue et al. (2009) because they yield similar thermometric  
532 results and thus could be distinguished by their precision, i.e. their sensitivity to the error  
533 factors. Starting from three Gulf Coast chlorite compositions (at 129, 204 and 232 °C as  
534 example), a Gaussian error distribution with  $1\sigma = 1\%$  relative for all oxides was randomly  
535 sampled around the nominal weight percentage for each oxide in chlorite. This deviation of  
536 1% for each oxide from the nominal composition was assumed to represent the TEM  
537 analytical uncertainties (as Vidal and Parra, 2000); 250 permutations led to the simulation of  
538 250 mineral compositions. The set of simulated chlorite compositions was used to calculate  
539 250 separate temperatures (noted “simulated temperatures”);  $\text{Fe}^{3+}$  content was recalculated  
540 each time. The maximum permissible scatter from the ‘nominal’ temperature estimate (from  
541 nominal chlorite) was fixed to a 95% confidence level. Indeed, 238 of the 250 simulated  
542 temperatures represent the assumed maximum temperature scatter, and therefore the influence  
543 of analytical uncertainties on temperature calculation. Results are presented in Figure 9. The  
544 observed variations of chemical compositions (Fig. 2 and 3) and the resulting variations of  
545 temperature estimates are clearly one order of magnitude larger than the possible effect of  
546 analytical uncertainties. For the Walshe (1986) model, 95% of simulated temperatures are  
547 separated by less than 10.7, 12.1 and 12.8 °C from the three nominal temperature estimates  
548 (190, 185 and 184 °C), respectively (Fig. 9). For the Vidal et al. (2005, 2006) model, the

549 absolute deviation is slightly higher than for the Walshe (1986) model, with 95% of simulated  
550 temperatures separated by less than 19, 17.4 and 14.8 °C from nominal temperature estimates  
551 (132, 211, 203 °C), respectively (Fig. 9). Finally, a higher absolute deviation of simulated  
552 temperatures is obtained for the Inoue et al. (2009) model, with 95% of simulated  
553 temperatures separated by a maximum of 15.7, 26.8 and 26.0 °C from nominal temperature  
554 estimates (143, 234, 235 °C), respectively (Fig. 9). These results show that the thermometer  
555 of Inoue et al. (2009) is the most sensitive to compositional variations, involving a  
556 dependence between the accuracy of analyses and that of the temperature calculation.  
557 Therefore, the relative accuracy (noted RA;  $RA = \text{absolute deviation represented by 95\% of}$   
558  $\text{simulated temperatures} \times 100 / \text{Estimated } T$ ) of the Inoue thermometer is consistently higher  
559 by more than 10.9%, whereas Vidal et al. (2005, 2006) model has a  $RA < 8.2\%$  (excepted for  
560  $BHT = 129 \text{ }^\circ\text{C}$ ) and Walshe (1986) model has a  $RA < 7\%$  (Fig. 9). Paradoxically, we observe  
561 that Walshe (1986) proposed a geothermometer with a very good reproducibility of estimates,  
562 but with a very rough accuracy. In fact, the best compromise between sensitivity to analytical  
563 uncertainties and accuracy of temperature is given by Vidal et al. (2005, 2006) model.

564

565 In the illite case, the empirical thermometer of Battaglia (2004) gives temperatures  
566 overestimated compared to the present-day temperatures. Remarks made against chlorite  
567 empirical thermometers are also valid in the illite case. Moreover, the equation correction  
568 involving  $|\text{Fe-Mg}|$ , as proposed by Battaglia (2004), has no crystal-chemical basis.

569 The temperatures estimated with the model of Dubacq et al. (2010) show the same increasing  
570 trend as measured temperatures and are not excessively scattered, especially at “high”- $T$  ( $>$   
571  $180 \text{ }^\circ\text{C}$ ). At lower temperature, the calculated temperatures may be overestimated by more  
572 than  $50^\circ\text{C}$ , but not systematically. This may be due to the difficulty to take into account  
573 purely potassic, charge-deficient 2:1 phyllosilicates at low- $T$ . The addition of  $\text{Fe}^{3+}$  content



574 deteriorates the correlation, and the estimated temperatures are slightly increased and  
575 scattered, involving a recommendation for a pure-Fe<sup>2+</sup> application as mentioned by the  
576 authors.

577

578         Concerning the illite-chlorite assemblage, the Walshe (1986) formalism for chlorite +  
579 mica + quartz + K-feldspar + water equilibrium yields calculated temperatures that are  
580 positively correlated with measured  $T$  (Fig. 7). For  $Fe_{total} = Fe^{2+}$ , this model allows one to  
581 obtain results with a better accuracy (50 °C on average) than those obtained with Walshe's  
582 chlorite + quartz thermometer, and the addition of Fe<sup>3+</sup> content changed the calculated  $T$  by  
583 only ~4 °C. The 'multi-equilibrium' approach combining Vidal et al. (2006) model for  
584 chlorite and Dubacq et al. (2010) model for smectite-illite-phengite gives plausible  
585 temperatures (Fig. 8): all temperatures boxes overlap the shaded area of BHT ± 50°C.  
586 However, several estimates yield too high temperatures, such as samples at 216 °C (BHT) for  
587 which the calculated  $T$  is overestimated, or one sample at 191 °C (BHT), for which the  
588 calculated  $T$  range is large (up to 339 °C). Nevertheless, the 'multi-equilibrium approach',  
589 combined to the fine-scale analytical protocol, gives satisfactory temperature estimates,  
590 showing the importance of analyses selection.

591 In summary, the two illite + chlorite models tested here give reliable results. In fact, the  
592 protocol enables to measure equilibrium compositions of both illite and chlorite at the  
593 nanoscale. These results suggest that it is likely the scale at which the heterogeneous  
594 equilibrium illite + chlorite is achieved. This allows for relating the different equilibrium  
595 compositions and gives a good basis for thermobarometry at low temperature.

596

597 **Chlorite and illite barometry**

598 The thermodynamic model of Vidal et al. (2005, 2006) is the only chlorite-based  
599 model to consider the pressure parameter. Applied to metamorphic rocks, it has shown the  
600 importance of pressure on the chemical composition variations (e.g. Malasoma and Marroni,  
601 2007). However, in a low- $P$ /low- $T$  diagram, the equilibrium curves calculated from our  
602 chlorite analyses are almost parallel to the  $P$  axis, which means that the chemical variations in  
603 chlorite are essentially dependent on temperature, thus confirming the validity of the  
604 assumption of Inoue et al. (2009). The model of Dubacq et al. (2010) considers the pressure  
605 as a significant parameter for the case of illite. Unlike the chlorite + quartz equilibrium curve,  
606 the illite + quartz equilibrium curve is not parallel to the  $P$  axis, and is  $P$ - $T$ -dependent.  
607 However, the  $dP/dT$  slope of this curve is steep, and for the  $P$ - $T$  domain investigated in this  
608 study, the model of Dubacq et al. (2010) predicts a higher  $T$ -dependence than  $P$ -dependence  
609 for illite composition. Moreover, the pressure uncertainty is as large as the entire range of  
610 pressure variations in diagenesis, which precludes any reliable estimate. Similarly, the  
611 pressure conditions constrained by the chlorite + illite equilibrium remain uncertain (Fig. 8-c),  
612 because of the steep slope of the illite + quartz equilibrium curve: except for one sample at  
613 1.05 kbar (BHP), all measured pressures are located in the calculated pressure ranges, but  
614 these ranges are large (up to 11 kbar). In fact, the pressure effect on the low- $T$  phyllosilicates  
615 appears to be too low compared to the temperature impact in this realm, involving a relative  
616 failure of the barometers to give results with acceptable error deviation.

617

618

### Concluding Remarks

619

620 The analytical protocol proposed by Bourdelle et al. (2012) makes it possible to obtain  
621 data at the nanometer scale and to distinguish crystal-rim and -core analyses, allowing one to  
622 analyse the illite-chlorite interfaces and the calculation of illite-chlorite equilibrium. In fact,

623 the difference of chemical composition between rims and cores may be very significant, in  
624 particular for the illite K content. Moreover, these chemical parameters generally show a  $T$ -  
625 dependence that is the base of many thermometers, making the consideration of chemical  
626 zonation a crucial point. In this respect, the present study showed the difference of impact and  
627 reliability for the two variables: temperature and pressure. The pressure does not affect the  
628 chlorite, but the illite composition. From the results of Vidal et al. (2005, 2006) and Dubacq et  
629 al. (2010) models, the chlorite + quartz equilibrium seems to be essentially  $T$ -dependent at  
630 low grade, whereas the illite + quartz equilibrium is influenced by both temperature and  
631 pressure. However, if the  $T$  estimate is realistic, the  $P$  prediction remains difficult and  
632 inaccurate.

633 Nevertheless, from a thermometric point of view, empirical and thermodynamic approaches  
634 lead to disparate results. The empirical chlorite thermometers all overestimate the temperature  
635 of the studied samples, because the  $T$ -dependent  $^{IV}Al$  or K variation alone is not an exclusive  
636 quantitative relation, and the common correction, based on  $X_{Fe}$ , does not improve the  
637 situation. The results of thermodynamic models are generally much more realistic (e.g. Vidal  
638 et al. 2005, 2006; Inoue et al. 2009; Dubacq et al. 2010 [in particular for  $T > 180$  °C], Walshe,  
639 1986 [for the chlorite + mica + quartz + K-feldspar + water equilibrium], and multi-  
640 equilibrium illite + chlorite approach), but revealed the importance of taking into account the  
641  $Fe^{3+}$  content, in particular in the case of chlorite disordered models.

642 The main difference between the semi-empirical or non-empirical thermodynamic and the  
643 empirical approaches is that the former are based on the ratio of chlorite end-members  
644 activities (equilibrium constant  $K$ ). The same  $\log K$ , and therefore the same temperature  
645 estimate can be obtained for chlorites of different compositions. Such approaches are thus  
646 compatible with the observation that chlorites crystallizing at the same temperature in rocks  
647 of different bulk compositions have different compositions. In contrast, such observation

648 cannot be accounted for by the empirical thermometers based on the <sup>IV</sup>Al content, even  
649 corrected using the Mg and Fe content (e.g. Karnidiotis and McLean 1987). Moreover,  
650 thermodynamic models make illite + chlorite thermometry possible in the low-*T* domain.  
651 Therefore, the chlorite + mica + quartz + K-feldspar + water thermometer proposed by  
652 Walshe (1986) and the combination of Dubacq et al. (2010) and Vidal et al. (2005, 2006)  
653 models give satisfactory results on Gulf Coast phyllosilicates, suggesting local equilibrium  
654 between illite and chlorite along crystal rims. The prerequisite for such results is that  
655 thermodynamic models are combined with an analytical technique that can resolve the very  
656 fine-scale compositional readjustments or overgrowths that may witness an approach of local  
657 equilibrium and keep a record of it. However, the choice of end-members for thermodynamic  
658 models can become a limitation depending on the composition domain studied. Indeed, the  
659 models of Vidal et al. (2005, 2006) and Walshe (1986) have the drawback to exclude many  
660 chlorite analyses with Si content higher or less than 3 apfu, respectively, which is  
661 unfortunately a common case for low-*T* chlorites.

662 Altogether, the thermodynamic approaches, based on the ratio of chlorite end-members  
663 activities, are compatible with the observation that chlorites crystallizing at the same  
664 temperature in rocks of different bulk compositions have different compositions. This study  
665 however stresses that recent models yield accurate results only if the compositional data used  
666 consider the chemical intracrystalline zonation occurring in low-*T* clay crystals. This requires  
667 the use of nanoscale chemical analysis.

668

669

670

## Acknowledgements

671

672 We are most grateful to the materials characterization department of IFP Energies nouvelles-  
673 Lyon, in particular to F. Moreau, and to the laboratory of CP2M-Université Aix-Marseille, for  
674 technical advice. Thanks are also extended to K. Milliken, S. Dutton and J. Donnelly of  
675 Bureau of Economic Geology at Austin. The discussions and comments of the journal editor  
676 R. Yuretich and of P. Aagaard are gratefully acknowledged. This study was financially  
677 supported by IFP Energies nouvelles, CNRS and ENS Paris.

678

## 679 **References**

680

681 Bailey, S.W. (1988) Chlorites: structures and crystal chemistry. In S.W. Bailey, Eds.,  
682 Hydrous Phyllosilicates (Exclusive of Micas), p. 347-403. Mineralogical Society of America,  
683 Washington D.C.

684 Battaglia, S. (2004) Variations in the chemical composition of illite from five geothermal  
685 fields: a possible geothermometer. *Clay Minerals*, 39, 501-510.

686 Bebout, D.G., Weise, B.R., Gregory, A.R., and Edwards, M.B. (1982) Wilcox sandstone  
687 reservoirs in the deep subsurface along the Texas Gulf Coast. 125 p. University of Texas,  
688 Austin.

689 Bodner, D.P. (1985) Heat variations caused by groundwater flow in growth faults of the  
690 South Texas, Gulf Coast basin, 187 p. Ph.D. thesis, University of Texas, Austin.

691 Bodner, D.P. and Sharp, J.M. (1988) Temperature variations in South Texas subsurface.  
692 *American Association of Petroleum Geologists Bulletin*, 72, 21-32.

693 Bourdelle, F. (2011) Thermobarométrie des phyllosilicates dans les séries naturelles:  
694 Conditions de la diagenèse et du métamorphisme de bas degré, 318 p. Ph.D. thesis, University  
695 Paris-Sud, Orsay.

696 Bourdelle, F., Parra, T., Beyssac, O., Chopin, C., and Moreau, F. (2012) Ultrathin section  
697 preparation of phyllosilicates by Focused Ion Beam milling for quantitative analysis by TEM-  
698 EDX. *Applied Clay Science*, 59-60, 121-130.

699 Cathelineau, M. (1988) Cation site occupancy in chlorites and illites as a function of  
700 temperature. *Clay Minerals*, 23, 471-485.

701 Cathelineau, M. and Nieva, D. (1985) A chlorite solid solution geothermometer. The Los  
702 Azufres (Mexico) geothermal system. *Contributions to Mineralogy and Petrology*, 91, 235-  
703 244.

704 De Caritat, P., Hutcheon, I., and Walshe, J.L. (1993) Chlorite geothermometry: a review.  
705 *Clays and Clay Minerals*, 41, 219-239.

706 Dodge, M.M. and Posey, J.S. (1981) Structural cross sections, Tertiary formations, Texas  
707 Gulf Coast. University of Texas, Austin.

708 Dubacq, B., Vidal, O., and De Andrade, V. (2010) Dehydration of dioctahedral aluminous  
709 phyllosilicates: thermodynamic modelling and implications for thermobarometric estimates.  
710 *Contributions to Mineralogy and Petrology*, 159, 159-174.

711 Dutton, S.P. and Loucks, R.G. (2010) Diagenetic controls on evolution of porosity and  
712 permeability in lower Tertiary Wilcox sandstones from shallow to ultradeep (200-6700 m)  
713 burial, Gulf of Mexico Basin, USA. *Marine and Petroleum Geology*, 27, 69-81.

714 Essene, E.J. and Peacor, D.R. (1995) Clay mineral thermometry - A critical perspective. *Clays*  
715 *and Clay Minerals*, 43, 540-553.

716 Heaney, P.J., Vicenzi, E.P., Giannuzzi, L.A., and Livi, K.J.T. (2001) Focused ion beam  
717 milling: A method of site-specific sample extraction for microanalysis of Earth and planetary  
718 materials. *American Mineralogist*, 86, 1094-1099.

719 Helgeson, H.C., Delany, J.M., Nessbitt, H.W., and Bird, D.K. (1978) Summary and critique  
720 of the thermodynamic properties of rock-forming minerals. *American Journal of Science*,  
721 278A, 1-229.

722 Helgeson, H.C and Aagaard, P. (1985) Activity/composition relations among silicates and  
723 aqueous solutions. I. Thermodynamics of intrasite mixing and substitutional order/disorder in  
724 minerals. *American Journal of Science*, 285, 769-844.

725 Hillier, S. and Velde, B. (1991) Octahedral Occupancy and the Chemical-Composition of  
726 Diagenetic (Low-Temperature) Chlorites. *Clay Minerals*, 26, 149-168.

727 Holland, T.J.B., Baker, J., and Powell, R. (1998) Mixing properties and activity composition  
728 relationships of chlorites in the system MgO-FeO-Al<sub>2</sub>O<sub>3</sub>-SiO<sub>2</sub>-H<sub>2</sub>O. *European Journal of*  
729 *Mineralogy*, 10, 395-406.

730 Hutcheon, I. (1990) Clay carbonate reactions in the Venture area, Scotian Shelf, Nova Scotia,  
731 Canada. *The Geochemical society, Special Publication*, 2, 199-212.

732 Inoue, A., Meunier, A., Patrier-Mas, P., Rigault, C., Beaufort, D., and Vieillard, P. (2009)  
733 Application of Chemical Geothermometry to Low-Temperature Trioctahedral Chlorites.  
734 *Clays and Clay Minerals*, 57, 371-382.

735 Jahren, J.S. (1991) Evidence of Ostwald ripening related recrystallization of chlorites from  
736 reservoir rocks offshore Norway. *Clay Minerals*, 26, 169-178.

737 Jahren, J.S. and Aagaard, P. (1989) Compositional variations in diagenetic chlorites and  
738 illites, and relationships with formation-water chemistry. *Clay Minerals*, 24, 157-170.

739 Jahren, J.S. and Aagaard, P. (1992) Diagenetic Illite-Chlorite Assemblages in Arenites .1.  
740 *Chemical Evolution. Clays and Clay Minerals*, 40, 540-546.

741 Jiang, W.T., Peacor, D.R., and Buseck, P.R. (1994) Chlorite Geothermometry -  
742 Contamination and Apparent Octahedral Vacancies. *Clays and Clay Minerals*, 42, 593-605.

743 Jones, P.H. (1975) Geothermal and hydrocarbon regimes, Northern Gulf of Mexico basin. In  
744 M.H. Dorfman and R.W. Deller, Eds., Proceedings of the first geopressed geothermal  
745 energy conference, p. 15-89. University of Texas, Center for energy studies, Austin.

746 Jowett, E.C. (1991) Fitting iron and magnesium into the hydrothermal chlorite  
747 geothermometer. GAC/MAC/SEG Joint annual meeting, Toronto, Canada.

748 Kehle, R.O. (1971) Geothermal survey of North America. Annual progress report, American  
749 Association of Petroleum Geologists, 31 p.

750 Kohler, E., Parra, T., and Vidal, O. (2009) Clayey Cap-Rock Behavior in H<sub>2</sub>O-CO<sub>2</sub> Media at  
751 Low Pressure and Temperature Conditions: An Experimental Approach. *Clays and Clay*  
752 *Minerals*, 57, 616-637.

753 Kisters, E.C., Bebout, D.G., Seni, S.J., Garrett, C.M., Brown, L.F., Hamlin, H.S., Dutton,  
754 S.P., Ruppel, S.C., Finley, R.J., and Tyler, N. (1989) Atlas of major Texas gas reservoirs. 168  
755 p. University of Texas, Austin.

756 Kranidiotis, P. and McLean, W.H. (1987) Systematics of chlorite alternation at the Phelps  
757 Dodge massive sulfide deposit, Matagami, Quebec. *Economic Geology*, 82, 1898-1911.

758 Lanson, B. and Besson, G. (1992) Characterization of the End of Smectite-to-Illite  
759 Transformation - Decomposition of X-Ray-Patterns. *Clays and Clay Minerals*, 40, 40-52.

760 Lieberman, J. and Petrakakis, K. (1991) TWEEQU Thermobarometry: Analysis of  
761 uncertainties and application to granulites from western Alaska and Austria. *Canadian*  
762 *Mineralogist*, 29, 857-887.

763 Loucks, R.G., Dodge, M.M., and Galloway, W.E. (1979) Sandstone consolidation analysis to  
764 delineate areas of high-quality reservoirs suitable for production of geopressed geothermal  
765 energy along the Texas Gulf Coast. 97 p. U.S. Department of energy, Austin.



766 Lynch, F.L. (1994) The effects of depositional environment and formation water chemistry on  
767 the diagenesis of Frio formation (Oligocene) sandstones and shales, Aransas, Nueces and San  
768 Patricio counties, Texas, 303 p. Ph.D. thesis, University of Texas, Austin.

769 Malasoma, A. and Marroni, M. (2007) HP/LT metamorphism in the Volparone Breccia  
770 (Northern Corsica, France): evidence for involvement of the Europe/Corsica continental  
771 margin in the Alpine subduction zone. *Journal of Metamorphic Geology*, 25, 529-545.

772 Mathieu, Y. and Velde, B. (1989) Identification of thermal anomalies using clay mineral  
773 composition. *Clay Minerals*, 24, 591-602.

774 McKenna, T.E. (1997) Geologic and hydrologic constraints on fluid and heat flow in  
775 overpressured rocks of the Rio Grande embayment, Gulf of Mexico basin, 241 p. Ph.D.  
776 thesis, University of Texas, Austin.

777 Nunn, J.A. (1984) Subsidence and temperature histories for Jurassic sediments in the  
778 Northern Gulf Coast: A thermal mechanical model. In D.G. Bebout, W.P.S. Ventress, B.F.  
779 Perkins and C.H. Moore, Eds., *The Jurassic of the Gulf rim*, p. 309-322. GCSSEPM  
780 Foundation 3th Annual Research Conference Proceedings, Houston, Texas.

781 Parra, T. (2001) Les équilibres chlorite-phengite : de l'étude de la lame mince aux calculs des  
782 trajets pression-température, 391 p. Ph.D thesis, Université Paris-Sud XI, Orsay.

783 Parra, T., Vidal, O., and Agard, P. (2002) A thermodynamic model for Fe-Mg dioctahedral K  
784 white micas using data from phase-equilibrium experiments and natural pelitic assemblages.  
785 *Contributions to Mineralogy and Petrology*, 143, 706-732.

786 Perry, E.A. and Hower, J. (1970) Burial diagenesis in Gulf Coast pelitic sediments. *Clays and*  
787 *Clay Minerals*, 18, 165-177.

788 Pfeiffer, D.S. (1989) Temperature variations and their relation to groundwater flow, South  
789 Texas, Gulf Coast basin, 198 p. Ph.D. thesis, University of Texas, Austin.

790 Posey, J.S. (1986) The Louann Salt of the Gulf Coast basin, with emphasis on South Texas. In  
791 W.L. Stapp, Eds., Contributions to the geology of South Texas, p. 440-446. South Texas  
792 Geological Society, San Antonio.

793 Royden, L., Sclater, J.G., and Von Her, R.P. (1980) Continental margin subsidence and heat  
794 flow: important parameters in formation of petroleum hydrocarbons. American Association of  
795 Petroleum Geologists Bulletin, 64, 173-187.

796 Shau, Y.H., Peacor, D.R., and Essene, E.J. (1990) Corrensite and mixed-layer  
797 chlorite/corrensite in metabasalt from northern Taiwan: TEM/AEM, EMPA, XRD and optical  
798 studies. Contributions to Mineralogy and Petrology, 105, 123-142.

799 Stanley, S.M. (1986) Earth and life through time, 689 p. New York.

800 Trotet, F., Vidal, O., and Jolivet, L. (2001) Exhumation of Syros and Sifnos metamorphic  
801 rocks (Cyclades, Greece): new constraints on the P-T paths. European Journal of Mineralogy,  
802 13, 901-920.

803 Van Cappellen, E. and Doukhan, J.C. (1994) Quantitative Transmission-X-Ray Microanalysis  
804 of Ionic Compounds. Ultramicroscopy, 53, 343-349.

805 Velde, B. and Medhioub, M. (1988) Approach to chemical equilibrium in diagenetic chlorites.  
806 Contributions to Mineralogy and Petrology, 98, 122-127.

807 Vidal, O., De Andrade, V., Lewin, E., Munoz, M., Parra, T., and Pascarelli, S. (2006) P-T-  
808 deformation-Fe<sup>3+</sup>/Fe<sup>2+</sup> mapping at the thin section scale and comparison with XANES  
809 mapping: application to a garnet-bearing metapelite from the Sambagawa metamorphic belt  
810 (Japan). Journal of Metamorphic Geology, 24, 669-683.

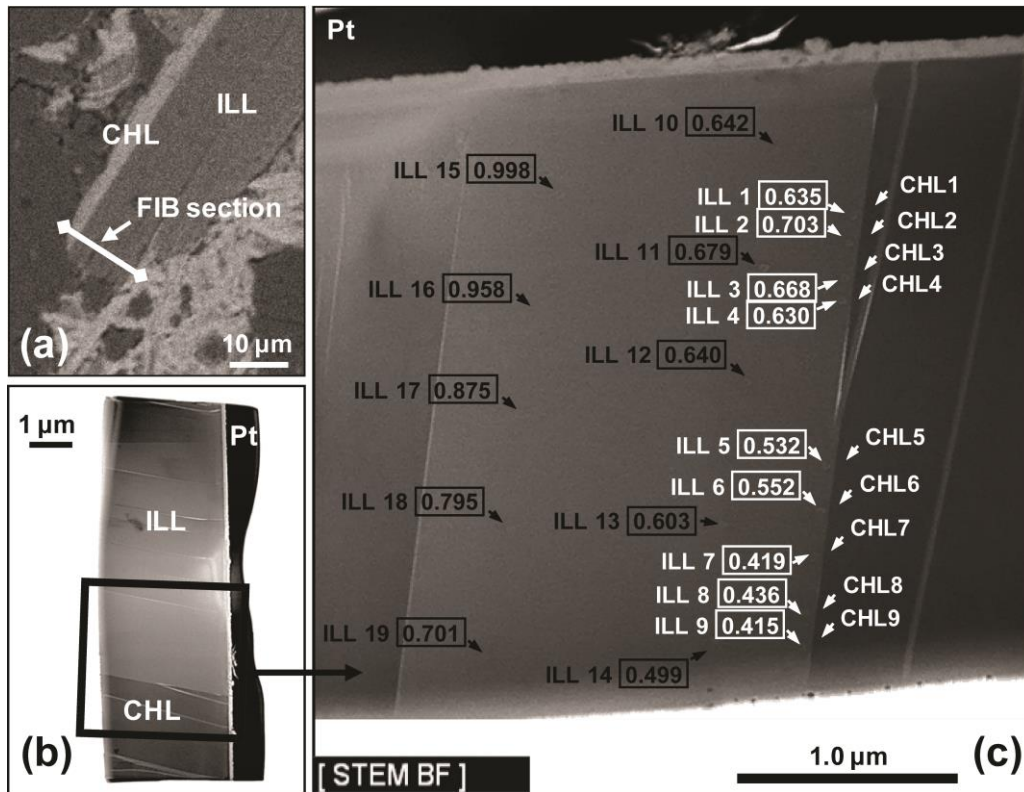
811 Vidal, O., Goffe, B., Bousquet, R., and Parra, T. (1999) Calibration and testing of an  
812 empirical chloritoid-chlorite Mg-Fe exchange thermometer and thermodynamic data for  
813 daphnite. Journal of Metamorphic Geology, 17, 25-39.

- 814 Vidal, O. and Parra, T. (2000) Exhumation paths of high-pressure metapelites obtained from  
815 local equilibria for chlorite-phengite assemblages. *Geological Journal*, 35, 139-161.
- 816 Vidal, O., Parra, T., and Trotet, F. (2001) A thermodynamic model for Fe-Mg aluminous  
817 chlorite using data from phase equilibrium experiments and natural pelitic assemblages in the  
818 100 ° to 600 °C, 1 to 25 kb range. *American Journal of Science*, 301, 557-592.
- 819 Vidal, O., Parra, T., and Vieillard, P. (2005) Thermodynamic properties of the Tschermak  
820 solid solution in Fe-chlorite: Application to natural examples and possible role of oxidation.  
821 *American Mineralogist*, 90, 347-358.
- 822 Walshe, J.L. (1986) A six-component chlorite solid solution model and the conditions of  
823 chlorite formation in hydrothermal and geothermal systems. *Economic Geology*, 81, 681-703.
- 824 Wirth, R. (2004) Focused Ion Beam (FIB): A novel technology for advanced application of  
825 micro- and nanoanalysis in geosciences and applied mineralogy. *European Journal of*  
826 *Mineralogy*, 16, 863-876.
- 827 Xie, X.G., Byerly, G.R., and Ferrell, R.E. (1997) I Ib trioctahedral chlorite from the Barberton  
828 greenstone belt: Crystal structure and rock composition constraints with implications to  
829 geothermometry. *Contributions to Mineralogy and Petrology*, 126, 275-291.
- 830 Zang, W. and Fyfe, W.S. (1995) Chloritization of the Hydrothermally Altered Bedrock at the  
831 Igarape-Bahia Gold Deposit, Carajas, Brazil. *Mineralium Deposita*, 30, 30-38.

832

833 **Figures**

834



835

836 Figure 1: Analysis of an illite-like - chlorite assemblage, sample of Alamo#1 well, 5825 m.

837 (a) SEM image of the petrographic thin section showing the emplacement of the FIB foil to be

838 cut across the illite-like - chlorite interface. (b) Brigh-field TEM image of the FIB foil

839 extracted from the section, with the platinum strap on top of it. (c) Enlargement with

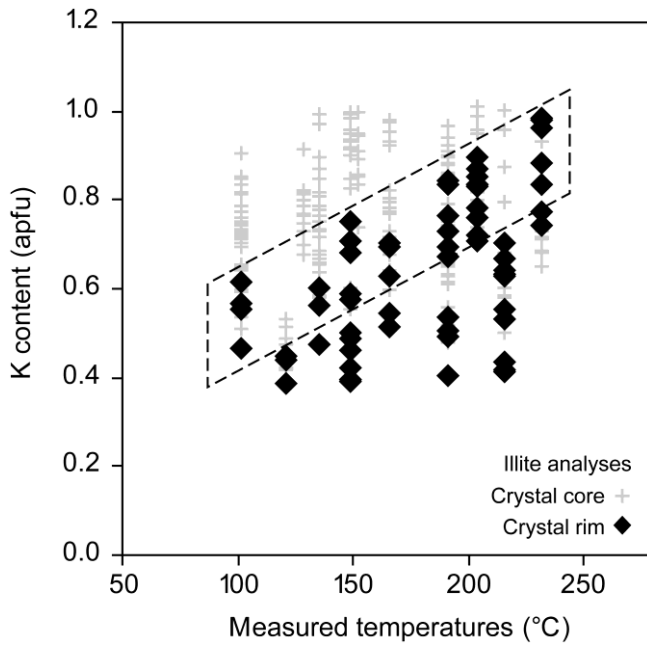
840 exaggerated image contrast in order to show the analysis points. Note their size as compared

841 to scale bar, and their distribution. Analyses 1 to 9 are considered as rim analyses [white text],

842 all others as core analyses [black text]. K contents are indicated for illite-like phase in apfu [in

843 boxes]. Note the K content variation between crystal core and crystal rim.

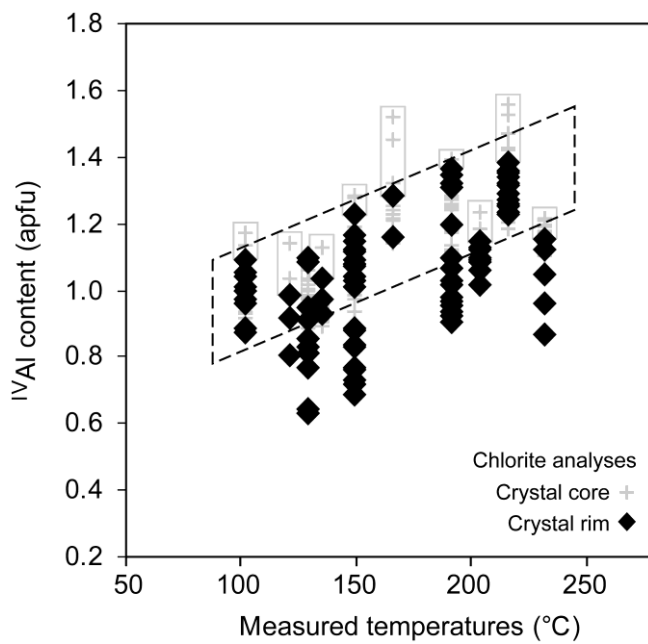
844



845

846 Figure 2: K contents of 2:1 phyllosilicates of Gulf Coast *versus* measured temperatures  
 847 (corrected bottom-hole temperature, BHT). Comparison of crystal-rim and crystal-core  
 848 analyses. The outlined area enclosed within dashed bands qualitatively underlines the trend  
 849 drawn approximately by the “maximum illitization”, i.e. rims analyses which were assumed  
 850 to represent the closest approach to relevant equilibrium composition.

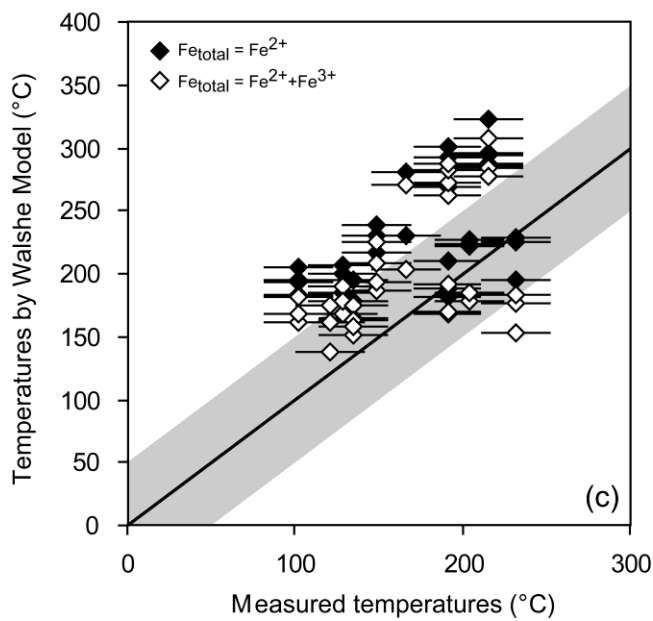
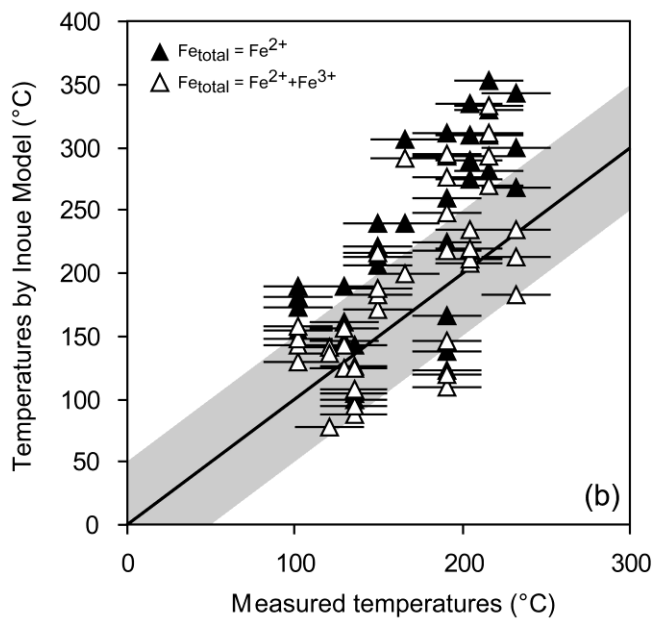
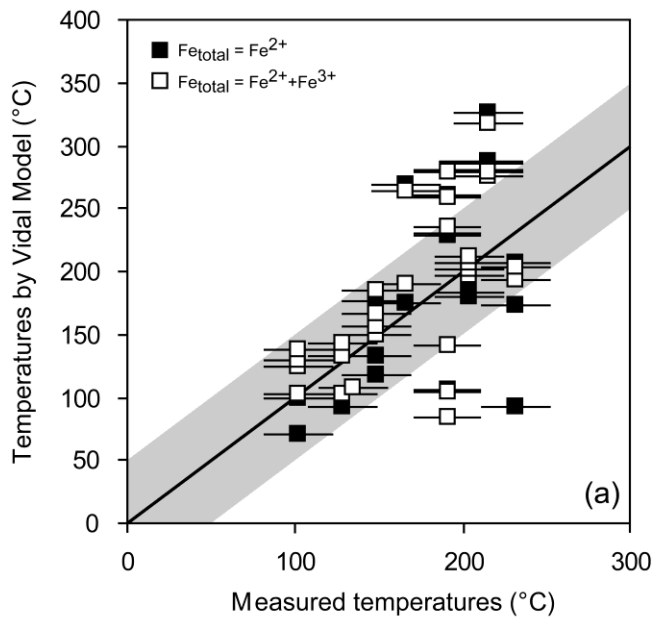
851



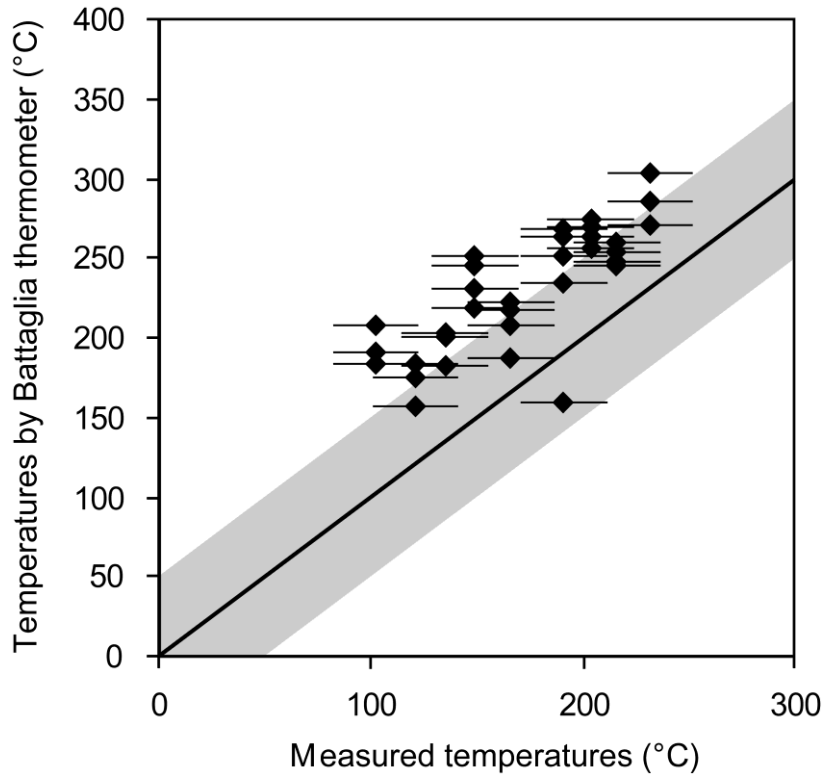
852

853 Figure 3:  $^{IV}Al$  contents of Gulf Coast chlorites *versus* measured temperatures (corrected  
854 BHT). Comparison of crystal-rim and crystal-core analyses. The outlined area enclosed  
855 within dashed band, qualitatively underlines the trend drawn approximately by the maximum  
856  $^{IV}Al$  content in crystal-rims, which is assumed to represent the closest approach to relevant  
857 equilibrium composition. Rectangles represent the difference between the maximum  $^{IV}Al$   
858 content in rims and cores of chlorite grains.

859

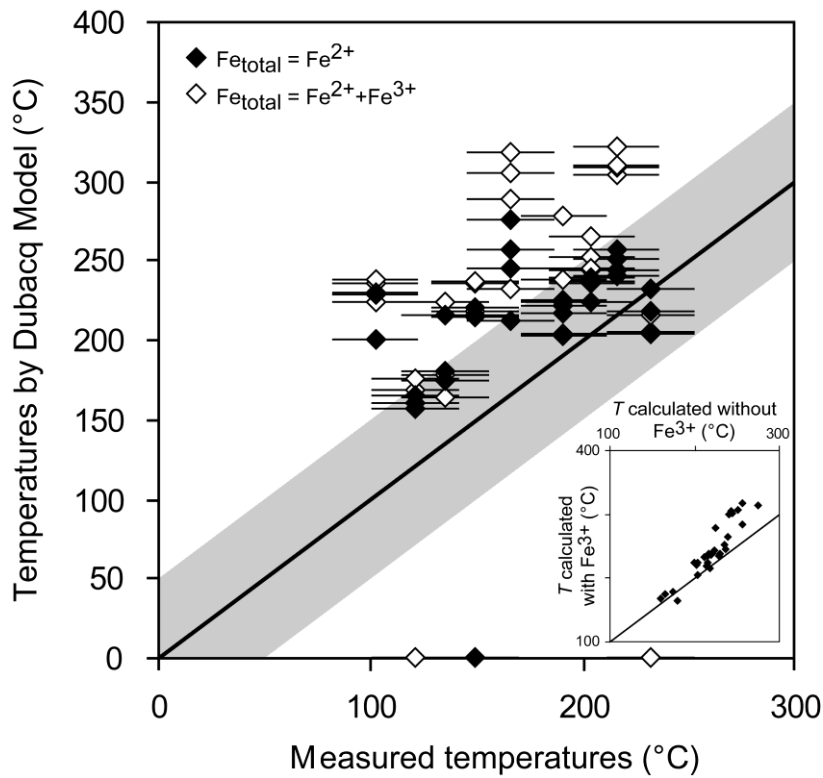


861 Figure 4: Comparison between measured temperatures (corrected BHT with an assumed error  
862 of 20 °C) and temperatures calculated with (a) Vidal et al. (2005, 2006) model, (b) Inoue et al.  
863 (2009) model and (c) Walshe (1986) model. Solid symbols,  $\text{Fe}_{\text{total}} = \text{Fe}^{2+}$ ; open symbols,  $\text{Fe}^{3+}$   
864 is considered (see text).  
865



866  
867 Figure 5: Comparison between measured temperatures (corrected BHT) and temperatures  
868 calculated with the empirical equation of Battaglia (2004). All Fe is considered as  $\text{Fe}^{2+}$ .  
869 Corrected BHT are represented with an assumed uncertainty of 20 °C.  
870

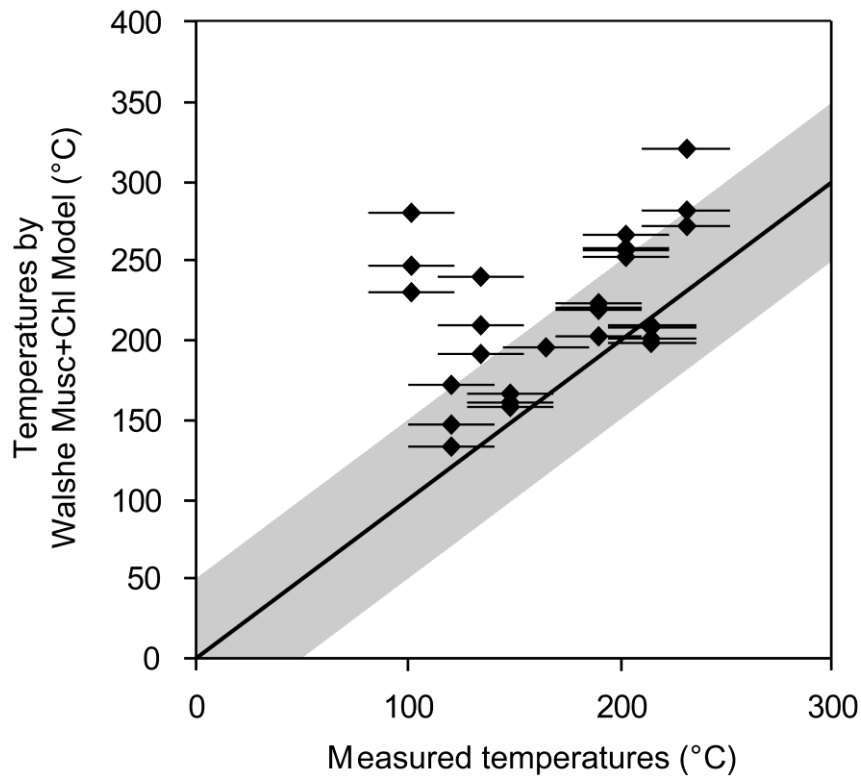




871

872 Figure 6: Comparison between measured temperatures (corrected BHT) and temperatures  
 873 calculated with the thermodynamic model of Dubacq et al. (2010). Solid symbols:  $Fe_{total} =$   
 874  $Fe^{2+}$ ; open symbols:  $Fe^{3+}$  content is considered (see text). Corrected BHT are represented with  
 875 an assumed uncertainty of 20 °C.

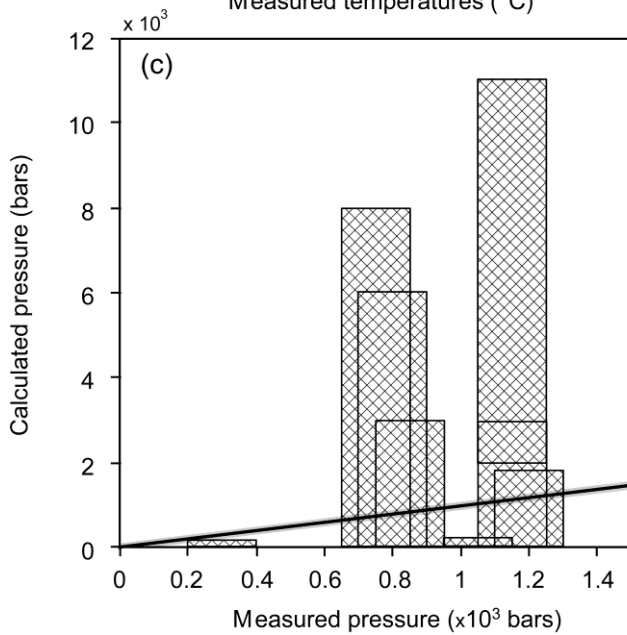
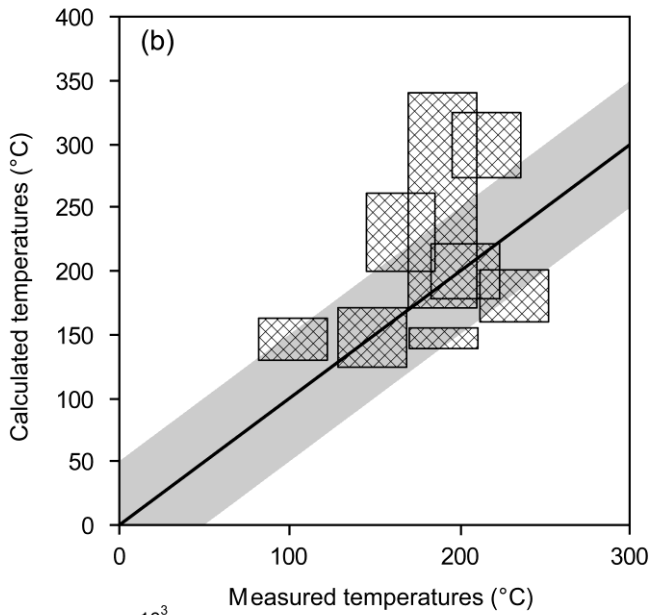
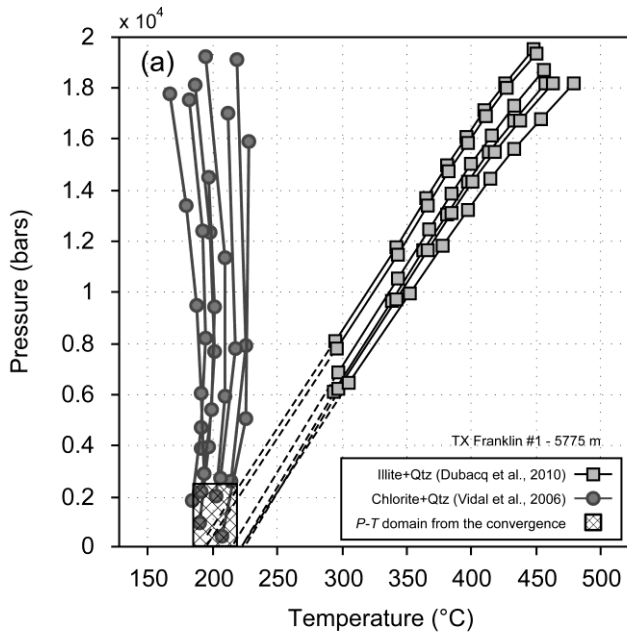
876



877

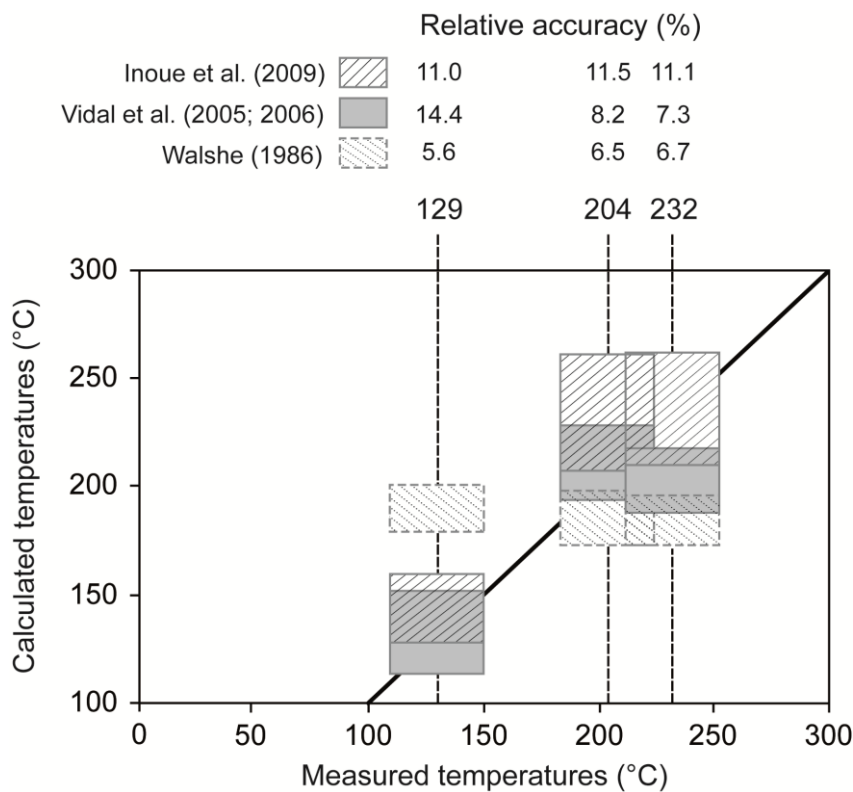
878 Figure 7: Comparison between measured temperatures (corrected BHT) and temperatures  
 879 calculated with the model of Walshe (1986) for the equilibrium chlorite + illite + K-feldspar +  
 880 quartz + water. All Fe is considered as Fe<sup>2+</sup>. Corrected BHT are represented with an assumed  
 881 uncertainty of 20 °C.

882



884 Figure 8: Temperatures and pressures obtained from the combination of the non-ideal ordered  
 885 models of Vidal et al. (2005, 2006) and Dubacq et al. (2010) for Gulf Coast chlorites. (a)  
 886 Example of equilibrium convergence for several chlorite and illite analyses of one Gulf coast  
 887 FIB section. The square area represents the  $P$ - $T$  domain of convergence. All chl-ill analysis  
 888 pairs are used. (b) Calculated temperatures compared to measured temperatures. Square areas  
 889 correspond to [in abscissa] the assumed uncertainty of 20 °C in BHT data, [in ordinate] the  
 890 maximum and the minimum temperatures obtained from the convergence domain (defined  
 891 from all chl-ill analysis pairs of all FIB sections for each  $P$ - $T$  data). (c) Calculated pressures  
 892 compared to measured pressures. Square areas correspond to [in abscissa] the assumed  
 893 uncertainty of  $\pm 100$  bars in BHP data, [in ordinate] the maximum and the minimum pressures  
 894 obtained from the convergence domain (defined from all chl-ill analysis pairs of all FIB  
 895 sections for each  $P$ - $T$  data).

896



897

898 Figure 9: Results in terms of temperature of the Monte-Carlo simulation for the three studied  
 899 chlorite thermometers (Walshe, 1986; Inoue et al., 2009; Vidal et al., 2005 2006), for three  
 900 nominal chlorites (at BHT = 129, 204 and 232 °C). The areas represent the assumed  
 901 uncertainty of  $\pm 20$  °C on BHT in abscissa and the absolute accuracy obtained from a Monte-  
 902 Carlo randomization on 250 chlorite compositions, with a 95% confidence level, in ordinate.  
 903 Relative accuracy corresponds to absolute deviation x 100 / Estimated  $T$ .

904

## 905 Tables

906

907 Table 1: Selection of TEM-EDX analyses of Gulf Coast K-deficient mica: crystal rim  
 908 analyses with the highest K content for each  $P$ - $T$ . Atomic contents are given in atoms per  
 909 formula unit (O = 11 apfu), and M1, M2 and M3 represent the cationic sites as defined by  
 910 Dubacq et al. (2010). All iron is considered as ferrous. The analytical uncertainties are  
 911 difficult to estimate, but are probably  $\pm 1$ -2 wt% for major elements and  $\pm 1$ -5 wt% for minor  
 912 elements (Bourdelle *et al.*, 2012); the impact of an uncertainty of  $\pm 1$  wt% (for each element)  
 913 on the thermometric estimations is discussed in the text.

914

Samples	AZ#159 9230	ST#470 10717	CK#2 12196	LA#1 13559	ST#356 14501	CW#1 14277	WR#C1 17805	FR#1 18946	AL#1 19110	AL#1 20711
Analysis	m42	m24	m24	m30	m13	m2	m33	m3	m34	M30
BHT (°C)	102	121	135	149	166	191	191	204	216	232
BHP (bars)	300	590	690	850	800	750	1050	1150	1150	1200
Si	3.38	3.78	3.44	3.41	3.10	3.43	3.37	3.30	3.18	3.32
Ti	0.01	0.01	0.01	0.02	0.02	0.00	0.03	0.02	0.00	0.02
<sup>IV</sup> Al	0.62	0.21	0.55	0.58	0.89	0.57	0.59	0.68	0.82	0.66
<sup>VI</sup> Al	1.87	1.53	1.82	1.75	1.86	1.90	1.48	1.57	1.74	1.59
$\Sigma$ Al	2.48	1.74	2.37	2.32	2.75	2.46	2.07	2.25	2.56	2.25
$\Sigma$ Fe <sup>2+</sup>	0.07	0.20	0.10	0.11	0.16	0.14	0.35	0.26	0.30	0.23
$\Sigma$ Mg	0.11	0.32	0.14	0.18	0.14	0.06	0.31	0.27	0.15	0.20
Mg (M1)	0.03	0.03	0.03	0.02	0.08	0.03	0.06	0.05	0.06	0.01
Fe <sup>2+</sup> (M1)	0.02	0.02	0.02	0.01	0.08	0.06	0.07	0.05	0.12	0.01
□(M1)	0.95	0.96	0.95	0.96	0.84	0.91	0.87	0.90	0.82	0.97
Mg (M2+M3)	0.08	0.29	0.10	0.16	0.07	0.03	0.24	0.22	0.08	0.19

Fe <sup>2+</sup> (M2+M3)	0.05	0.18	0.08	0.10	0.07	0.07	0.28	0.21	0.17	0.22
K	0.62	0.45	0.60	0.75	0.70	0.40	0.84	0.90	0.70	0.99
Na	0.04	0.03	0.03	0.00	0.00	0.05	0.00	0.00	0.00	0.03
Ca	0.00	0.06	0.00	0.00	0.00	0.02	0.00	0.00	0.00	0.00
v	0.35	0.46	0.37	0.25	0.30	0.53	0.16	0.10	0.30	0.00

915

916 Table 2: Selection of TEM-EDX analyses of Gulf Coast chlorites: crystal rim analyses with  
917 the highest <sup>IV</sup>Al content for each *P-T*. Atomic contents are given in atoms per formula unit  
918 (O=14 apfu), and M1, M2, M3 and M4 represent the cationic sites as defined by Vidal et al.  
919 (2005, 2006). All iron is considered as ferrous, value in bold indicates an analysis excluded by  
920 Vidal's model (Si > 3 apfu). The analytical uncertainties are difficult to estimate, but are  
921 probably ±1-2 wt% for major elements and ±1-5 wt% for minor elements (Bourdelle *et al.*,  
922 2012); the impact of an uncertainty of ±1 wt% (for each element) on the thermometric  
923 estimations is discussed in the text.

924

Sample	AZ#159 9230	ST#470 10717	CK#2 11924	CK#2 12196	LA#1 13559	ST#356 14501	CW#1 14277	WR#C1 17805	FR#1 18946	AL#1 19110	AL#1 20711
Analysis	chl28	chl30	chl50	chl20	chl23	chl34	chl31	chl16	chl29	chl25	chl29
BHT (°C)	102	121	129	135	149	166	191	191	204	216	232
BHP (bars)	300	590	660	690	850	800	750	1050	1150	1150	1200
Si	2.91	<b>3.01</b>	2.90	2.96	2.88	2.71	2.63	2.90	2.84	2.61	2.85
Ti	0.00	0.01	0.01	0.00	0.00	0.00	0.01	0.00	0.01	0.00	0.00
<sup>IV</sup> Al	1.09	0.98	1.09	1.03	1.12	1.28	1.37	1.10	1.15	1.38	1.15
<sup>VI</sup> Al	1.77	1.79	1.89	1.82	1.79	1.71	1.84	1.85	1.50	1.78	1.48
ΣAl	2.86	2.77	2.98	2.85	2.91	3.00	3.21	2.95	2.64	3.16	2.64
ΣFe <sup>2+</sup>	2.46	2.53	2.37	2.45	3.28	2.07	3.01	2.48	2.15	2.44	2.93
ΣMg	1.39	1.22	1.31	1.34	0.53	1.98	0.85	1.28	2.11	1.55	1.36
Mg (M1)	0.22	-	0.19	0.20	0.08	0.26	0.09	0.18	0.36	0.17	0.23
Fe <sup>2+</sup> (M1)	0.39	-	0.35	0.37	0.52	0.27	0.32	0.36	0.37	0.27	0.51
Al (M1)	0.09	-	0.09	0.03	0.12	0.28	0.37	0.10	0.15	0.38	0.15
□(M1)	0.29	-	0.37	0.39	0.27	0.19	0.22	0.36	0.12	0.17	0.11
Mg (M2+M3)	1.17	-	1.12	1.14	0.44	1.72	0.76	1.09	1.75	1.38	1.12
Fe <sup>2+</sup> (M2+M3)	2.07	-	2.03	2.08	2.76	1.80	2.69	2.12	1.78	2.17	2.43
Al (M2+M3)	0.67	-	0.79	0.78	0.66	0.43	0.48	0.75	0.35	0.40	0.33
Al (M4)	1.00	-	1.00	1.00	1.00	1.00	1.00	1.00	1.00	1.00	1.00
XFe <sup>3+</sup>	0.28	0	0.23	0.28	0.20	0.05	0.05	0.22	0.36	0.05	0.27

925

926 Table 3: Clay thermometry models tested in this study.

927

Model	Type	Variables	Assumptions	Other components
<i>Chlorite models</i>				
Cathelineau and Nieva (1985)	Empirical	$T$	$^{IV}Al$ increase with $T$	
Walshe (1986) (1)	Thermodynamic	$T$	Chl+qz equilibrium	Random cation mixing
Kranidiotis and McLean (1987)	Empirical	$T$	$^{IV}Al$ increase with $T$	Correction of bulk composition effect from Fe/(Fe+Mg)
Cathelineau (1988)	Empirical	$T$	$^{IV}Al$ increase with $T$	
Jowett (1991)	Empirical	$T$	$^{IV}Al$ increase with $T$	Correction of bulk composition effect from Fe/(Fe+Mg)
Hillier and Velde (1991)	Empirical	$T$	$^{IV}Al$ increase with $T$	
Zang and Fyfe (1995)	Empirical	$T$	$^{IV}Al$ increase with $T$	Correction of bulk composition effect from Fe/(Fe+Mg)
Xie et al. (1997)	Empirical	$T$	$^{IV}Al$ increase with $T$	Correction of bulk composition effect from Fe/(Fe+Mg)
Vidal et al. (2006)	Thermodynamic	$T$ - $P$	Chl+qz including non-ideality	Ordered cation mixing
Inoue et al. (2009)	Thermodynamic	$T$	Chl+qz	Random cation mixing Semi-empirical equation
<i>Illite/mica-like models</i>				
Battaglia (2004)	Empirical	$T$	K increase with $T$	Correction of bulk composition effect from  Fe-Mg
Dubacq et al. (2010)	Thermodynamic	$T$ - $P$ hydration	Mica-like+qz including non-ideality	Ordered cation mixing
<i>Illite+chlorite models</i>				
Walshe (1986) (2)	Thermodynamic	$T$	Chl+mica+qz+feldspar	Random cation mixing
Vidal et al. (2006) + Dubacq et al. (2010)	Thermodynamic	$T$ - $P$	Multi-equilibrium	Ordered cation mixing